Andean Geology 38 (2): 284-318. Julio, 2011

Andean Geology
formerly Revista Geológica de Chile
www.andeangeology.cl

Low-grade metamorphism of Cambro-Ordovician successions in the Famatina belt, Southern-Central Andes: Burial-inversion history linked to the evolution of the proto-Andean Gondwana margin

Gilda Collo[1], Margarita Do Campo[2], Fernando Nieto[3]

[1] *Laboratorio de Análisis de Cuencas, CICTERRA-Universidad Nacional de Córdoba, Av. Vélez Sarsfield 1611, 2° piso, of. 7, X5016GCA Córdoba, Argentina.*
gcollo@efn.uncor.edu

[2] *Instituto de Geocronología y Geología Isotópica, Facultad de Ciencias Exactas y Naturales, Universidad de Buenos Aires, Pabellón INGEIS, Ciudad Universitaria, 1428 Buenos Aires, Argentina.*
marga@ingeis.uba.ar

[3] *Departamento de Mineralogía y Petrología, Instituto Andaluz de Ciencias de la Tierra, Universidad de Granada-CSIC, Avda. Fuentenueva s/n, 18002 Granada, Spain.*
nieto@ugr.es

ABSTRACT. The metamorphic P-T conditions of low-grade units from the Famatina belt, Central Andes of Argentina, were estimated through petrography, X-ray diffraction, and electron microscopy. For the Middle-Upper Cambrian Negro Peinado Formation a tectono-metamorphic event associated with intense intrafoliar folding, with estimated temperatures between 290 and 400°C (KI_{CIS}: 0.16-0.27Δº2θ, biotite blastesis and compositional homogeneity in dioctahedral micas) and intermediate pressure conditions (white mica *b* parameter: 9.010Å-9.035Å), was recognized. The Achavil Formation (Middle-Upper Cambrian) presents a main metamorphic event associated with temperatures between 200 and 290°C (KI_{CIS}: 0.26-0.41Δº2θ) and intermediate- to low-pressure conditions (white mica *b* parameter values: 8.972Å-9.017Å). Some illitic substitution in dioctahedral micas also indicates lower metamorphic grade than the Negro Peinado Formation. For Upper Cambrian to Middle Ordovician sequences a burial metamorphic pattern, with a progressive decrease in metamorphic grade from Volcancito Formation to Cerro Morado Group (*ca.* 490-465 Ma; KI_{CIS}: 0.31-0.69Δº2θ) and absence of tendency changes linked to stratigraphic discontinuities was proposed. Mica and chlorite are the main phyllosilicates in the oldest units, while Ilt/Sme (R3) mixed-layer is almost the only one in the youngest. White mica *b* parameter indicates intermediate- to low-pressure conditions for all these sequences. This burial metamorphic pattern presents a marked break as the youngest Ordovician unit (La Aguadita Formation, after *ca*. 452 Ma) records higher metamorphic conditions (IK_{CIS}: 0.28-0.19Δº2θ) than units from the Ordovician arc, with estimated temperatures between 270 and 330ºC and intermediate-pressure conditions. Our results indicate that basin contraction and inversion processes related to the Ordovician Ocloyic Orogeny involved at least two well-discriminated and not superposed metamorphic episodes in this region.

Keywords: Western Gondwana margin, Ocloyic orogeny, Famatina belt, Low-grade metamorphism.

RESUMEN. Metamorfismo de bajo grado de sucesiones cambro-ordovícicas en el cinturón del Famatina, Andes Centrales de Argentina: Historia de enterramiento-exhumación ligada a la evolución del margen proto-andino de Gondwana. Las condiciones P-T del metamorfismo de las unidades de bajo grado del cinturón del Famatina, Andes Centrales de Argentina, fueron estimadas mediante petrografía, difracción de rayos-X y microscopía electrónica. La Formación Negro Peinado (Cámbrico Medio-Superior) fue afectada por un evento tectono-metamórfico asociado con un plegamiento intrafoliar intenso, para el cual se estimaron temperaturas entre 290 y 400°C (IK_{CIS}: 0,16-0,27 Δº2θ, blástesis de biotita y homogeneidad composicional en micas dioctaédricas) y presiones intermedias (parámetro *b* de la mica blanca: 9,010 Å y 9,035 Å). La Formación Achavil (Cámbrico Medio-Superior) presenta un evento metamórfico asociado con temperaturas entre 200 y 290°C (KI_{CIS}: 0,26-0,41Δº2θ) y condiciones de presión intermedias-bajas (parámetro *b* de la mica blanca: 8,972Å-9,017Å). Para las sucesiones comprendidas entre el Cámbrico Superior y el Ordovícico Medio, se identificó un patrón metamórfico de soterramiento, con una disminución progresiva en el grado metamórfico desde la Formación Volcancito hasta el Grupo Cerro Morado (*ca*. 490-465 Ma; IK_{CIS}: 0,31-0,69 Δº2θ) y ausencia de cambios de tendencia ligados a las discontinuidades estratigráficas. La mica blanca y la clorita son los principales filosilicatos en las unidades más antiguas, mientras los interestratificados Ilt/Sme (R3) son casi exclusivos en las más jóvenes. El parámetro *b* de la mica blanca indica condiciones de presión intermedia-baja para estas unidades. Este patrón metamórfico de soterramiento presenta un marcado quiebre hacia la unidad ordovícica más joven (Formación La Aguadita, posterior a los *ca*. 452 Ma) con temperaturas estimadas entre 270 y 330°C (IK_{CIS}: 0,28-0,19Δº2θ) y condiciones de presión intermedias. Nuestros resultados indican que los procesos relacionados con la contracción e inversión de la cuenca durante la orogenia Oclóyica involucran en esta región al menos dos episodios metamórficos bien diferenciados y no superpuestos.

Palabras clave: Margen occidental de Gondwana, Orogenia Oclóyica, Cinturón de Famatina, Metamorfismo de bajo grado.

1. Introduction

The Famatina belt, in the Central Andean Region of Argentina (Fig. 1), is part of an ancient subduction-collisional margin that formed along western Gondwana during the Early Palaeozoic (Vaughan and Pankhurst, 2008). Within this belt, Middle-Upper Cambrian to Middle-Upper Ordovician deposits constitute an almost continuous succession affected by low-grade metamorphism. The well-constrained and mostly preserved Cambro-Ordovician stratigraphy in this region allows the reconstruction of the sedimentary history related to the evolution of the Ocloyic arc (Astini, 2003; Astini and Dávila, 2004). Three major stages of sedimentation record the period preceding the initiation of subduction up to the uplift and basin inversion in the final stages of the Ocloyic

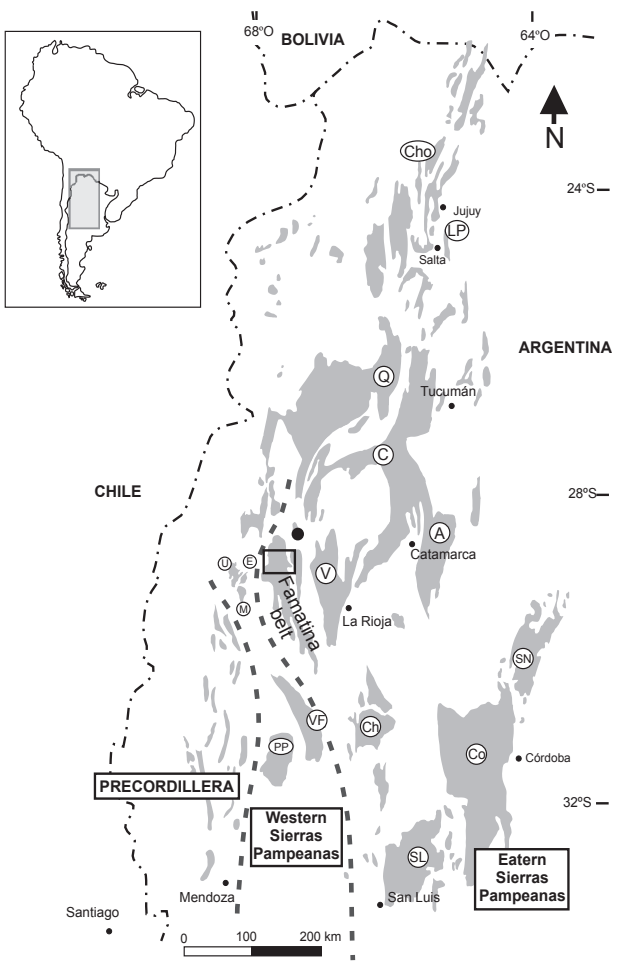

FIG. 1. Location map with distribution of main mountain ranges of the Central Southern Andes (Western Argentina): **LP**: Lules-Puncoviscana belt; **Cho**: Choromoro belt; **Q**: Sierra de Quilmes; **C**: Capillitas; **A**: Ancasti; **V**: Velazco; **E**: El Espinal; **U**: Umango; **M**: Sierra de Maz; **VF**: Valle Fértil; **PP**: Pie de Palo; **Ch**: Chepes and Llanos de La Rioja; **SL**: Sierras de San Luis; **Co**: Sierras de Córdoba; **SN**: Sierra Norte. Bold dashed lines show boundaries between main geological provinces. The black box indicates the location of the detailed area in figure 3.

orogeny, which has been commonly related with the collision of the Precordillera terrane from the west (*ca*. 460 Ma). The earliest stage started with the deposition of the Middle-Upper Cambrian synorogenic units, the Negro Peinado and Achavil Formations, deposited in a peripheral foreland that developed during the final stages of the Pampean orogeny (Pampean synorogenic suite, *ca*. 520-500 Ma; Fig. 2; Collo and Astini, 2008; Collo *et al*., 2009). A second stage comprises the sequences associated with the initiation of an east-dipping subduction regime to the west, and the concomitant development of the Ordovician Ocloyic magmatic arc (Astini, 2003), including volcanic units representing two main volcanic episodes (Fig. 2). The latest depositional stage is recorded by the Upper Ordovician La Aguadita Formation (after *ca*. 452 Ma), that would correspond to a foreland basin, synorogenic with the Ocloyic orogeny, and mainly sourced by the Ocloyic granitoids (Ocloyic synorogenic suite, *ca*. 480-460 Ma, Fig. 2; Astini *et al*., 2005; Rapela *et al*., 1998; Dahlquist *et al*., 2005).

U-Pb geochronology from the region (Rapela *et al*., 2007; Collo *et al*., 2009), together with K-Ar analyses (Collo *et al*., 2008), indicate that, contrary to long-held belief, the post-depositional history and the related low-grade metamorphism of the Cambro-Ordovician units are entirely associated with the Ordovician Ocloyic orogeny. Medium- to high-grade metamorphism linked to this orogeny is well described in rocks cropping out east-southeast of the study region (cf. Steenken *et al*., 2004; 2006; Delpino *et al*., 2007; Verdecchia, 2009), suggesting the existence of low-pressure metamorphism coupled with back-arc extension and subsequent closure of the basins.

With the aim of understanding the post-depositional history of the diverse low-grade metamorphic units within the Famatina belt, their thermobarometric conditions were first constrained through petrographic and mineralogical analyses. Subsequent detailed SEM analysis identified metamorphic reactions not previously observed through optical microscopy and XRD analyses, and also determined mineral chemistry at the micron scale. The results showed that the youngest Ordovician unit of the easternmost back-arc region records higher metamorphic conditions than the older units within the Ordovician arc (Collo *et al*., 2005; Collo and Astini, 2008). Although low-grade patterns evidencing metamorphic inversion are common, they are mainly recorded within forearc regions between trenches and accretionary prisms, where the younging-upward increase in metamorphic grade is the result of progressively older overriding strata. This seems not to be the case of the studied successions genetically linked to a continental arc setting (Astini, 2003).

In this contribution, we present the set of data obtained, together with a discussion of the geodynamic evolution of the subduction-collisional margin of western Gondwana during the Cambro-Ordovician at these latitudes, as it emerges from the assemblage of petrographic, geochronological, microtectonic, and structural information. The uniqueness of the volcano-sedimentary Cambro-Ordovician record at Famatina belt also makes this a key region for understanding complex subsidence-burial mechanisms that occurred at the higher structural levels within the Ocloyic Orogeny, whose post-depositional history has mainly been established through the study of middle- to high-grade metamorphic units.

2. Low-grade rocks from Famatina belt

The low-grade units from Famatina belt crop out in different tectonic sheets associated with the Andean uplift and affected by intensive shortening. The Negro Peinado Formation (Middle-Upper Cambrian) crops out as a relatively continuous central sheet (Las Trancas sheet) without stratigraphic contacts with Lower Palaeozoic units (Fig. 3a). Its low-grade metamorphism is associated with tight isoclinal folding, with the S_1 foliation parallel to the S_0 and sandstone levels boudinated within pelitic layers. Most of the remaining Cambro-Ordovician rocks crop out in two central-western sheets (Los Damascos and Los Colorados sheets; Fig. 3a). Within these sheets, the Achavil Formation (Middle-Upper Cambrian; Collo, 2006; Collo and Astini, 2008) is unconformably overlain by the Cambro-Ordovician Volcancito Formation and the subsequent well-known Ordovician volcano-sedimentary successions (over 4,000 m in thickness) comprising the Bordo Atravesado Formation, the Cerro Tocino Volcanics, and the Famatina and Cerro Morado groups (Fig. 3b). Although this volcaniclastic sequence clearly preserves its sedimentary attributes, it is also affected by low-grade metamorphism (Toselli and Weber, 1982; Collo, 2008). The Achavil Formation records complex folding associated with the oldest strain events identified in the region. It is the result of the superposition of two

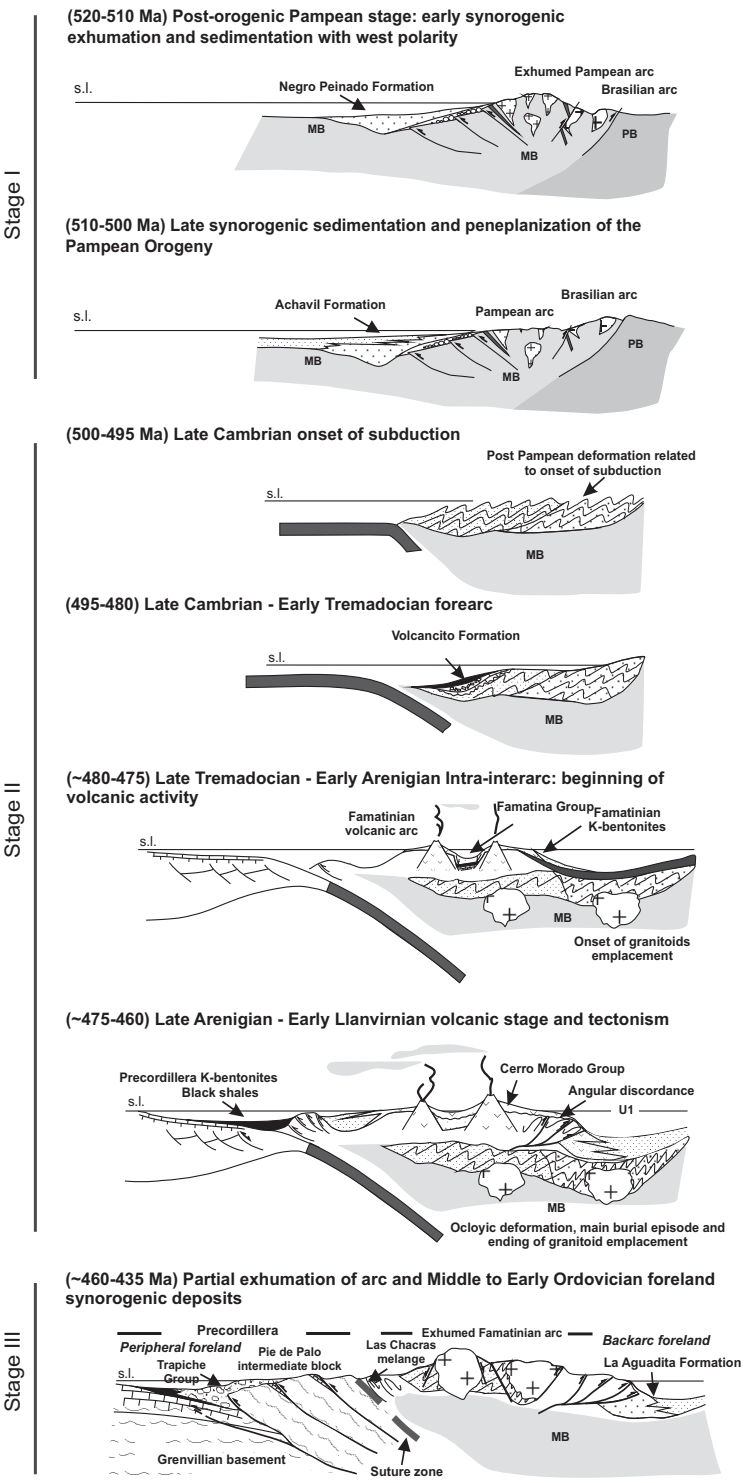

FIG. 2. Evolution of Famatinian Cambro-Ordovician units within the Ocloyic Orogeny as proposed by Astini *et al*. (2007), Astini and Dávila (2004), and Collo *et al*. (2009).

different deformational stages, a N-S compressive phase and a further E-W com-pressive phase ($P1_{ACH}$ and $P2_{ACH}$), probably linked to the onset of subduction in the western margin of Gondwana during the Upper Cambrian (Collo *et al*., 2006). The discordance between the Achavil and Volcancito Formations could also be correlated with the Iruyic discordance identified in NW Argentina between the Mesón and Santa Victoria groups (Astini *et al*., 2005). An east-verging fold-thrust belt associated with the Ocloyic orogeny itself is evidenced by the angular unconformity between the Early Ordovician Famatina Group and the overlying Ordovician Cerro Morado Group, both part of the anticline of Los Colorados in the central Famatina belt (Dávila *et al*., 2003; Astini and Dávila, 2002).

The youngest La Aguadita Formation crops out in a small, independent eastern sheet (Valle de la Aguadita sheet; Fig. 3a) and, as with the Negro Peinado Formation, there is no stratigraphic relation between this unit and the other Cambro-Ordovician sequences. Petrologic, mineralogical (XRD), and textural analyses (Collo *et al*., 2005) of metasandstones and metapelites from the Loma de las Damas outcrop indicate that the rocks were affected by a regional low-grade metamorphic-deformational episode whose main blastesis was contemporary with the development of the S_1 foliation.

3. Analytical methods

3.1. XRD analysis

Samples for clay mineral X-ray analysis were prepared following the recommendations of Moore and Reynolds (1997).

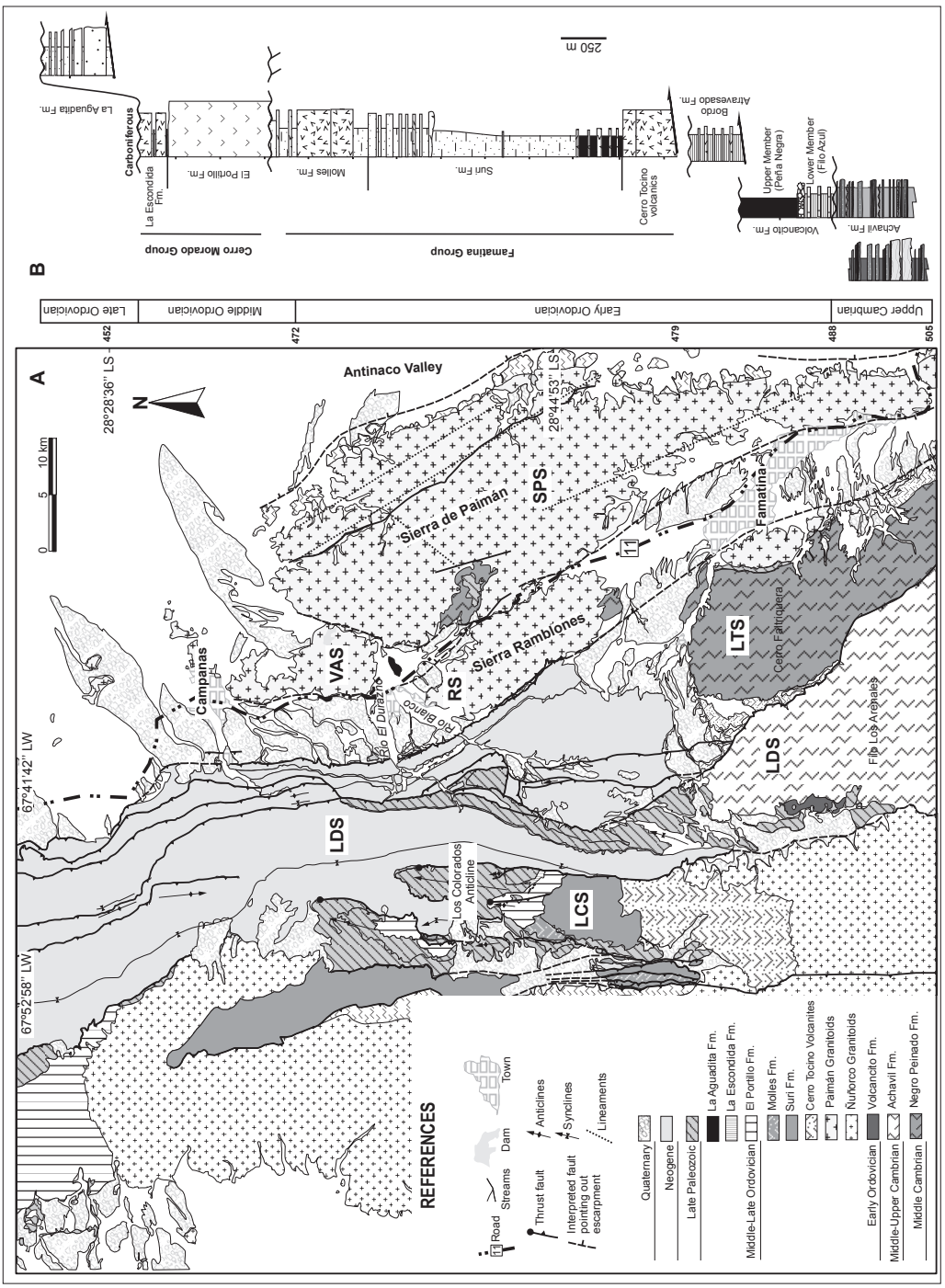

FIG. 3. **A.** Geological map of the central region of the Famatina belt (modified from Dávila and Astini, 2007). **VAS**: Valle La Aguadita thrust sheet; **SPS**: Sierra de Paimán thrust sheet; **RS**: Ramblones thrust sheet; **LTS**: Las Trancas thrust sheet; **LDS**: Los Damascos thrust sheet; **LCS**: Los Colorados thrust sheet; **B.** Cambro-Ordovician stratigraphy within the Famatina belt (modified from Astini and Dávila, 2004).

The <2 μm fraction was separated for 17 pelitic samples. Clay-mineral composition was established by the comparison of orientated aggregates that were air-dried (AO), ethylene-glycol solvated (EG), and heated at 500ºC (HO). X-ray analyses were determined with Philips PW1050 (INGEIS) and X-Pert Pro (Departamento de Físico-Química-UNC) diffractometers, employing Cu radiation from 4 to 30º2θ with a step size of 0.03º2θ and a count time of 0.5 s per step. Clay-mineral phases were semi-quantified using MIF factors and the recommendations of Moore and Reynolds (1997). The Kübler Index (KI) was measured in both AO and EG orientated aggregates, and CIS values (Crystallinity Index Standard, Warr and Rice, 1994) were established from the regression equation for the Philips PW1050 diffractometer: y=1.2175x+0.0833 (R^2=0.975). In samples with evidence of smectite or illite/smectite mixed-layer (hereafter Ilt/Sme), $KI_{(CIS)}$ measurements were carried out on the 5Å illite reflection in EG-treated aggregates in order to avoid the influence of expandable layers. $KI_{(CIS)}$ values were only measured in rocks without blastic biotite. The white mica *b* parameter (Guidotti and Sassi, 1986) was measured in rock slices orientated perpendicular to the main foliation, and the quartz (211) reflection positioned at 1.541Å was used as internal standard. Mineral abbreviations proposed by Whitney and Evans (2010) were used.

3.2. Scanning and transmission electron microscope

Fifteen metapelitic levels belonging to the Negro Peinado, Achavil, and La Aguadita formations were analysed by scanning electron microscopy (Zeiss DSM950 SEM and Variable Pressure SEM) and a Philips CM-20 scanning transmission electron microscope (STEM) equipped with an ultra-thin window EDX detector (Centro de Instrumentación Científica, Granada University). The main goal was to understand the mineralogical and textural evolution of low-grade rocks in Famatina belt, first constrained through petrography and XRD (Kübler index, white mica *b* parameter). Further goals were to characterize the chemical composition of phyllosilicate minerals and to fix geobarometric constraints (Massone and Szpurka, 1997). These three units were chosen as they recorded the highest metamorphic grades. For textural analysis, backscattered electron images were used, whereas the chemical composition of phyllosilicates was established through EDX on carbon-coated polished samples studied by SEM and through analytical electron microscopy (AEM) in Au grids under TEM. Quantitative AEM analyses were obtained from thin edges using a 1000x200Å scanning area. Counting times of 15 s and 100 s minimized alkali-loss problems as short counting times improve reproducibility for K^+ and Na^+ (Nieto *et al*., 1996). Standards used to obtain the K-factors for the transformation of intensity ratios to concentration were albite, biotite, spessartine, muscovite, olivine, and titanite (following the methods of Cliff and Lorimer, 1975 and Champness *et al*., 1981). Mica compositions were established from samples with and without biotite blastesis. The structural formulae of dioctahedral micas were calculated considering 22 negative charges and 0.25 to 0.50 Fe^{2+}/Fe^{3+} ratios depending on the iron-bearing phases present in individual samples (or in each unit) (cf. Guidotti *et al*., 1994). Mica formulae showing Mg^{++} contents higher than (Si-3) were considered to be contaminated with chlorite, whereas data showing anomalously low interlayer charges and high Si contents were interpreted as being contaminated with quartz. Both groups of data were discarded. Chlorite formulae were calculated considering 28 negative charges and ferrous iron (Fe^{2+}). Small amounts of K^+, Na^+, and Ca^{++} identified in some chlorites from both units were interpreted as indicative of mica contamination; in such cases, compositions were corrected following the recommendations of Nieto (1997).

4. Results

4.1. Petrography, clay mineralogy, and crystal-chemical indices

4.1.1. Negro Peinado Formation (Middle-Upper Cambrian)

This unit mainly comprises blackish-green phyllites alternating with centimetric levels of metasandstones (metawackes and subordinate metaarkoses; Fig 4a). Fine-grained white mica, chlorite, quartz, and feldspars are the principal phases in all phyllites from this sequence (Fig. 4b and c), with associated biotite blastesis in some localities. These minerals define a zonal to continuous spaced me-

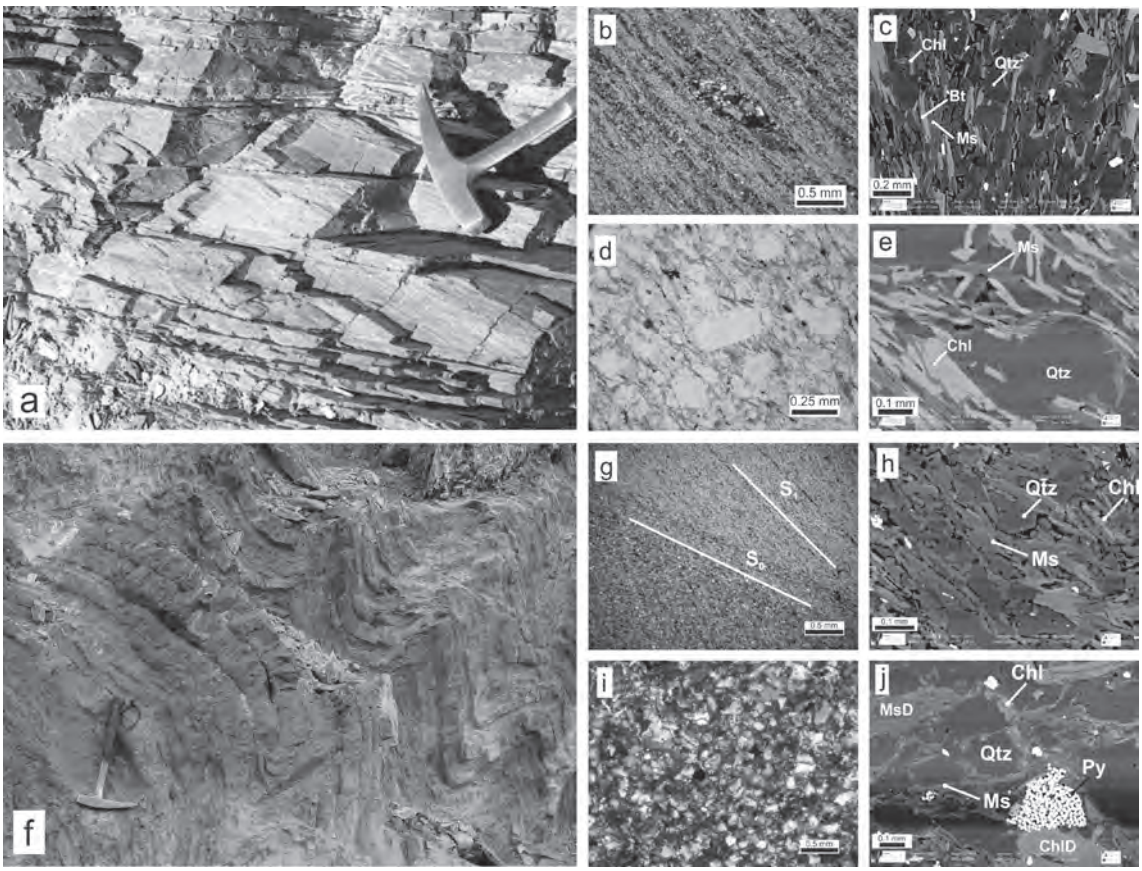

FIG. 4. The Negro Peinado Formation. **a.** Outcrop view of the sequence showing millimetric alternance of silty-sandy and shale layers; **b.** and **c.** Metapelites showing development of P and Q domains coincident with the metamorphic S_1 foliation (c: BSE image). Mica, chlorite, and blastic biotite grains are commonly larger than 50 mm and appear as orientated crystals (0.01 to 0.02 mm long) surrounding quartz grains (0.05 to 0.1 mm). Quartz generally appears as elongated grains, with sutured-serrated to straight edges, occasionally with undulatory extinction; **d.** and **e.** Metasandstones, see the sutured to serrated contacts and the beard quartz-feldspar grains surrounded by a phyllosilicate matrix defining the metamorphic foliation S_1 (e: BSE images). White mica is very thin (0.02 mm) and occasionally forms interleaved phyllosilicate grains with chlorite and biotite, elongated parallel to the metamorphic foliation, but with individual crystal (001) planes perpendicular to S_1. Chlorite is wider than mica (0.05 to 0.1 mm), tabular, and intensely green; it presents variable interference colours, from intense blue to brown, indicating compositional variations within individual samples, from magnesian-chamosite to ferrous-clinochlore, respectively (cf. Nieto, 1997). Sometimes quartz grains are broken and displaced, with the fractures filled by chlorite crystals with the (001) planes oblique to the metamorphic foliation. The Achavil Formation; **f.** outcrop view of the sequence showing the alternance of shales and sandy levels and folding; **g.** and **h.** Metapelites with oblique sedimentary S_0 and metamorphic S_1 foliations (h: BSE image). Subrounded opaque minerals, occasionally as aggregates, and biotite and mica detrital grains were also observed. Chlorite frequently replaces detrital biotite grains; **i.** and **j.** Quartzose metasandstones with sutured contact between quartz grains and undulatory extinction (j: BSE image).

tamorphic foliation (S_1) mainly subparallel to the sedimentary layering (S_0), with a lepidoblastic to lepidogranoblastic texture depending on the millimetric compositional-granulometric layering. P and Q domains are well developed. Occasionally very thin sandy layers are folded within the fine-grained domains. Intergrown muscovite-biotite grains are also common. Metawackes are mainly composed of quartz and plagioclase with minor amounts of K-feldspar (Fig. 4d and e). Lepidogranoblastic domains are mainly formed by orientated phyllosilicates, although quartz grains are abundant. Blastic biotite, when present, appears as thin flakes and is commonly intergrown with chlorite. In granoblastic domains, quartz (0.05 to 0.6 mm) is sigmoidal or eye-shaped, with undulatory extinction; it also

presents subgrains and sutured to serrated contacts. In these domains, the phyllosilicates surround quartz and feldspar grains that frequently develop beards and pressure shadows associated to the S_1 foliation. Meta-arkoses are mainly composed of quartz-feldspathic grains (84% quartz and 16% plagioclase, according to XRD analyses) with scarce matrix.

The clay fraction from fine-grained levels mainly consists of mica (~50-90%) and chlorite (~10-50%), with scarce smectite and the sporadic appearance of interstratified illite-smectite. In one sample, a 7Å phase (identified by its reflections at 7.15Å and 3.57Å) was interpreted as kaolinite (Table 1). Changes in chlorite composition between samples were infered through XRD analyses, as variable height ratios of odd and even basal reflections suggest variable total Fe contents.

$KI_{(CIS)}$ values measured in five biotite-free samples range between 0.28 and 0.16ºΔ2θ, belonging to the upper anchizone-epizone fields transition (Table 1). KI values, together with the biotite blastesis registered in several samples, indicates temperatures between 290 and 400°C. The white mica *b* parameter gave a mean value of 9.021Å (n: 13, s: 0.009), consistent with intermediate-pressure facies metamorphism according to Guidotti and Sassi (1986). Most of the values range between 9.010Å and 9.035Å, with the two lower values (9.004Å and 9.005Å) corresponding to samples with biotite blastesis (see samples CH64 and CH73 in Appendix A), reflecting the lower phengitic substitution in white micas from biotite-muscovite associations (Ernst, 1963) related with the reaction: phengite+chlorite→muscovite+ biotite+quartz+water.

4.1.2. The Achavil Formation (Middle-Upper Cambrian)

This unit constitutes a relatively homogeneous to highly rhythmic stratified sequence of green to dark grey dominantly shales with millimetric compositional-granulometric layering (Fig. 4f). The pelite/sandstone thickness ratio is generally over 10, and exceptionally some micro-conglomeratic levels are preserved. Primary features are generally obliterated by neoformation and transformation processes that give rise to blastopelitic to lepidogranoblastic textures. In metapelites (Fig. 4g and h), neoformed fine-grained white mica and chlorite (<0.01 mm) surround thin quartz-feldspathic grains defining smooth metamorphic foliation (cf. Passchier and Trouw, 1998) subparallel to oblique to the sedimentary layering. SEM images depict muscovite and chlorite neoformed grains, seldom larger than 10 μm. Sandy levels (Fig. 4i and h) are lighter in colour than pelites, they correspond to quartzose sandstones to quartzose metawackes generally having millimetric parallel to cross-layering. They have a blastopsamitic texture with quartz grains up to 0.13 mm in size, exhibiting undulatory extinction and sutured to serrated contacts, and subordinate plagioclase and lithic fragments. Scarce neoformed phyllosilicates (fine-grained white mica and chlorite) are orientated parallel to S_0. The development of metamorphic foliation is not clear within these levels. Common Fe-bearing phases are pyrite, as ehuedral crystals and framboidal aggregates, and ilmenite; sometimes they are replaced by oxidized secondary Fe phases. The XRD analyses of clay fractions indicate higher mica abundances in Achavil (~68-98%) than in the Negro Peinado Formation metapelites (Table 1), whereas chlorite represents a subordinate phase (2-32%). Despite the mineralogical homogeneity of most of the samples, two diagrams present a group of low-intensity reflections in the heat-treated aggregates (500ºC) at ~15.8, 7.8, 4.2, and 3.8Å, probably corresponding to interstratified chlorite/vermiculite (Chl/Vrm). Moreover, one sample presents traces of smectite (4%). $KI_{(CIS)}$ values range between 0.41 and 0.26ºΔ2θ (n: 11), indicating that these rocks were buried under low- to upper-anchizone conditions (Merriman and Peacor, 1999), with temperatures of around 200 to 290°C. The white mica *b* parameter, measured in eight samples, shows a mean value of 9.009 Å with a standard deviation of 0.005 (Table 1).

4.1.3. Volcaniclastic units (Upper Cambrian-Middle Ordovician)

4.1.3.1. The Volcancito Formation

This unit is formed by two contrasting members. The lower calcarenitic member (Lower Member, cf. Astini, 2003) is characterized by the presence of carbonate intraclasts (mudstones) with inclusions of siliceous spicules and bioclasts (Nuia, Girvanella, pelmatozoa, trilobites, brachiopods, ostracods, gastropods; Astini, 2001, 2003), all surrounded by sparitic cement. It also contains abundant quartz

TABLE 1. INTEGRATED TABLE WITH DATA FROM ALL THE ANALYSED UNITS. KÜBLER INDEXES AND WHITE MICA *b* PARAMETER VALUES CONSIDERED IN EACH UNIT ARE SHOWN IN BOLD. SEE TEXT FOR FURTHER EXPLANATIONS.

		MINERALOGY										IK		*b* parameter	
	Sample	**Ilt**	**Chl**	**Sme**	**Berthierine**	**Kln**	**Vrm**	**Ilt/Sme**	**Ilt/Chl**	**Chl/Vrm**	**Bt**	**CIS(AD)**	**CIS(EG)**	**CIS range**	***b***	***b mean***
La Aguadita Formation	Lag	61	4	3	X	-	-	33	-	-	-	0.32	0.31		-	
	LD1p	92	5	3	-	-	-	-	-	-	-	0.40	0.40		9.028	
	LD2p	-	-	-	-	-	-	-	-	-	X	-	-		9.026	9.024
	LD3p	88	7	5	-	X	-	-	-	-	-	0.29	-	0.28-0.40	-	
	LD6p	89	9	3	-	-	X	-	-	-	-	0.30	0.28		9.022	n:4
	LD6a	-	-	-	-	-	-	-	-	-	-	-	-	n:6	9.026	
	LD7p	75	8	3	X	-	X	-	14	-	-	0.29	0.29		9.020	s:0.004
	LD8p	90	8	2	-	-	-	-	-	X	-	0.34	0.34		-	
	LD9p	94	-	6	-	-	-	-	-	-	X	-	-		9.023	
La Escondida Formation	LE1	-	-	-	-	-	X	100	-	-	-	0.83	0.69	0.5 -0.69	-	
	LE7	-	-	-	-	2	X	98	-	-	-	0.69	0.64		-	
	CM5	-	-	-	-	4	-	96	-	-	-	0.68	0.50	n:3	-	
Molles Formation	CM-32	99	1	-	-	-	-	-	-	-	-	0.84	-		-	
	CM-40	-	-	-	-	-	-	100	-	-	-	1.43	1.32	0.46-1.32	-	
	LMA2	92	8	-	-	-	-	-	-	-	-	0.55	-		-	
	LMA115	89	11	-	-	-	-	-	-	-	-	0.46	-	n:5	-	
	M2	90	10	-	-	-	-	-	-	-	-	0.54	-		-	9.011
Suri Formation	S1	89	11	-	-	-	-	-	-	-	-	0.52	-		-	n:4
	S2	80	20	-		-	-	-	-	-	-	0.48	-		-	
	S4	76	24	-	-	-		-	-	-	-	0.51	-		-	s: 0.006
	S5	82	18	-	-	-	-	-	-	-	-	0.51	-		-	
	S6	80	20	-	-	-	X	-	18	-	-	0.59	-	0.41-0.59	-	
	S7	76	24	-	-	-	-	-	-	-	-	0.53	-		-	
	S8	80	20	-	-	-	-	-	-	-	-	0.48	-	n: 15	-	
	S10	97	3	-	-	-	-	-	-	X	-	0.53	-		-	
	S12	95	5	-	-	-	X	-	-	-	-	0.51	-		-	
	S13	95	5	-	-	-	-	-	-	X	-	0.53	-		-	
	S18	97	3	-	-	-	-	-	-	-	-	0.52	-		-	

Table 1 continued.

		MINERALOGY										IK		*b* parameter	
	Sample	**Ilt**	**Chl**	**Sme**	**Berthierine**	**Kln**	**Vrm**	**Ilt/Sme**	**Ilt/Chl**	**Chl/Vrm**	**Bt**	**CIS(AD)**	**CIS(EG)**	**CIS range**	***b***	***b mean***
Suri Formation	S22	90	10	-	-	-	-	-	-	-	-	0.46	-		-	
	S23	-	-	-	-	-	-	-	-	-	-	0.41	-		-	
	QS5	100	-	-	-	-	-	-	-	-	-	0.55	-		-	9.011
	SC	92	8	-	-	-	-	-	-	-	-	0.42	-	0.41-0.59	-	n:4
	QS1	-	-	-	-	-	-	-	-	-	-	-	-	n: 15	9.015	s: 0.006
	QS33	-	-	-	-	-	-	-	-	-	-	-	-		9.003	
	QSp8	-	-	-	-	-	-	-	-	-	-	-	-		9.015	
	Sch	-	-	-	-	-	-	-	-	-	-	-	-		9.012	
Bordo Atravesado Formation	BA	95	5	-	-		X	-	-	X	-	0.35	-	0.31-0.35	-	
	BA1D	90	10	-	-		X	-	-	X	-	0.31	-	n:2	-	
Volcancito Formation	AC-V	77	-	2	21	-	-	-	-	-	-	0.41	0.38		-	
	PS1	90	-	10	-	-	-	-	-	-	-	0.44	0.34		-	
	PS2	93	5	2	-	-	-	-	-	-	-	0.37	0.38		-	
	QV1a	93	7	-	X	-	-	-	-	X	-	0.34	-		-	
	QV1b	89	11	-	-	-	X	-	-	-	-	0.36	-		-	
	QV1c	91	9	-	-	-	-	-	-	-	-	0.38	-		9.026	
	QV2	78	4	-	-	-	-	-	18	-	-	0.39	-	0.33-0.39	-	9.018
	QV3	92	8	-	-	-	-	-	-	-	-	0.37	-	n:15	-	n:4
	QV4	80	20	-	-	-	-	-	-	-	-	0.38	-		9.017	s:0.006
	QV5	79	21	-	-	-	-	-	-	-	-	0.35	-		9.020	
	QV6a	85	15	-	-	-	-	-	-	-	-	0.39	-		-	
	QV6b	95	5	-	-	-	-	-	-	-	-	0.37	-		-	
	QV6c	77	23	-	-	-	-	-	-	-	-	0.34	-		-	
	QV7	88	12	-	-	-	-	-	-	-	-	0.35	-		9.011	
	QV9	-	-	-	-	-	-	-	-	-	-	0.33	-		-	
Achavil Formation	AA1	85	15	-	-	-	-	-	-	-	-	0.41	-		-	
	AA2	72	28	-	-	-	-	-	-	-	-	0.37	-	0.26-0.41	-	9.009
	V5m	92	8	-	-	-	-	-	-	X	-	0.34	-	n:11	9.011	n:8
	V10	99	1	-	-	-	-	-	-	-	-	-	-		-	s:0.005
	V11	87	13	-	-	-	-	-	-	X	-	0.27	-		-	

Table 1 continued.

		MINERALOGY										IK			*b* parameter	
	Sample	**Ilt**	**Chl**	**Sme**	**Berthierine**	**Kln**	**Vrm**	**Ilt/Sme**	**Ilt/Chl**	**Chl/Vrm**	**Bt**	**CIS(AD)**	**CIS(EG)**	**CIS range**	***b***	***b mean***
Achavil Formation	V12	84	13	4	-	-	-	-	-	-	-	0.41	0.34		9.013	
	V13	96	4	-	-	-	-	-	-	-	-	0.39	-		-	
	V14	83	17	-	-	-	-	-	-	-	-	0.38	-		-	
	V15	75	25	-	-	-	-	-	-	-	-	0.40	-		9.006	9.009
	V15a	-	-	-	-	-	-	-	-	-	-	-	-	0.26-0.41	9.011	n:8
	V16	79	21	-	-	-	-	-	-	-	-	0.39	-	n:11	9.017	s:0.005
	ACH	-	-	-	-	-	-	-	-	-	-	0.26	-		9.006	
	546	-	-	-	-	-	-	-	-	-	-	-	-		8.972	
	547	-	-	-	-	-	-	-	-	-	-	0.27	-		-	
	Q Ach	-	-	-	-	-	-	-	-	-	-	-	-		9.01	
Negro Peinado Formation	NP2	49	42	10	-	-	-	-	-	-	-	0.24	0.20		9.027	
	NP3	54	-	4	44	-	-	-	-	-	-	0.24	0.23		9.026	
	NP4	-	-	-	-	-	-	-	-	-	-	-	-		9.030	
	NP5	-	-	-	-	-	-	-	-	-	-	-	-		9.024	
	NP11	-	-	-	-	-	-	-	-	-	-	-	-		9.016	
	NP12	-	-	-	-	-	-	-	-	-	-	-	-		9.023	
	CH73	-	-	-	-	-	-	-	-	-	X	-	-		9.005	
	CH64	-	-	-	-	-	-	-	-	-	-	-	-		9.010	
	Pl	-	-	-	-	-	-	-	-	-	-	-	-		9.020	9.021
	QP	-	-	-	-	-	-	-	-	-	-	-	-	0.16-0.28	9.026	n:13
	QP3a	-	-	-	-	-	-	-	-	-	-	-	-	n:5	9.035	s:0.009
	QP4	67	33	-	-	-	-	-	-	-	-	0.27	-		-	
	QP6a	-	-	-	-	-	-	-	-	-	-	-	-		9.026	
	QP6p	-	-	-	-	-	-	-	-	-	-	-	-		9.021	
	QP7p	-	-	-	-	-	-	-	-	-	-	-	-		9.014	
	CNP	-	-	-	-	-	-	-	-	-	X	-	-		9.004	
	CNP2	63	36	1	-	-	-	X	-	-	X	0.30	0.16		-	
	CH55	-	-	-	-	-	-	-	-	-	-	-	-		-	
	517	-	-	-	-	-	-	-	-	-	-	-	-		-	

and plagioclase grains, quartzose metamorphic lithoclasts, opaque minerals, zircon, chlorite, and subordinate muscovite. The intraclasts and some bioclasts (predominantly pelmatozoa) are broken, crushed, and rotated, with fractures filled by calcite and, occasionally, folded. Stylolites depicting concentrations of less soluble phases (clay, iron oxides, and organic matter), and orientated parallel to the S_0 primary foliation, were also identified. In levels where the carbonate cement is not abundant, quartz grains present sutured to plane contacts, and some concave-convex contacts involving clay-silt intraclasts. Pyrite is the most abundant opaque mineral, and appears as framboidal aggregates, but also as irregular and euhedral crystals (nano- and micropyrite; Brand, 2004; Schoonen, 2004). Clay minerals associated with the carbonate cement include white mica and chlorite. Sometimes radial chlorite surrounds pyrite grains and replaces some framboidal aggregates. In addition, there are multiple fractures, post-dating most of the aforedescribed diagenetic features, filled with calcite, quartz, and opaque minerals. In this member, fine-grained rocks show millimetric S_0 compositional layering, with alternating light quartz-rich bands and dark bands with higher organic matter and phyllosilicatic contents.

The upper pelitic member (Upper Member, cf. Astini, 2003; Fig. 5a and b) is mainly formed of shales with distinct parallel lamination and composed predominantly of quartz, plagioclase, organic matter, opaque minerals, fine-grained white mica, chlorite, and isolated intraclasts. The neoformed phyllosilicates are orientated parallel to the S_0. Interlayered with these dominant pelitic levels are fine to medium (0.07 to 0.1 mm) quartz-sandstone levels and scarce intraclastic mudstone and conglomerate levels. The sandstones have quartz grains with plane, sutured to serrated contacts, lithic fragments, feldspar, opaque minerals (predominantly euhuedral

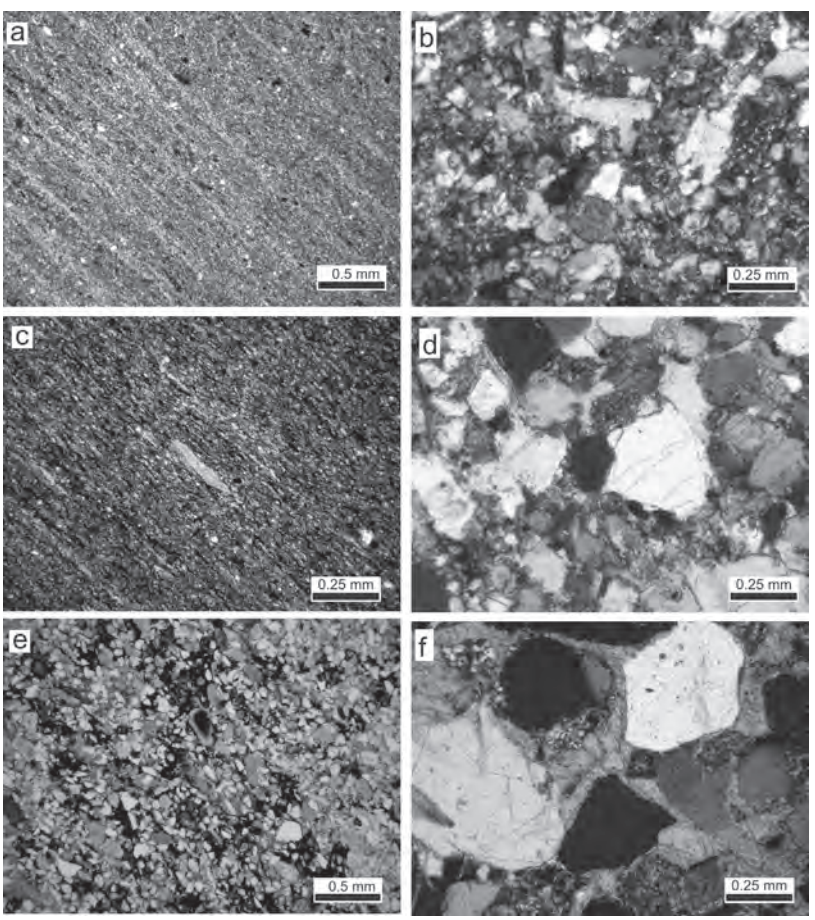

FIG. 5. The Volcancito Formation: **a.** Metapelite with development of secondary foliation parallel to the sedimentary layering; **b.** Metasandstone with quartz overgrowths in optical continuity and plane to sutured contacts. The Suri Formation: **c.** Metapelites with argillaceous mineral growth parallel to sedimentary layering; **d.** Metasandstone with abundant quartz grains showing overgrowths in optical continuity and plane to concave-convex contacts. The Molles Formation: **e.** Volcaniclastic sandstone with abundant subrounded and embayed quartz grains; **f.** Detail showing carbonate cement surrounding quartz overgrowths.

and framboidal pyrite), and intergrown chlorite and mica grains in a quartz-micaceous matrix with abundant chlorite and scarce carbonate cement (micrite). Some levels within this member have haematitic aggregates, probably generated at the expense of the dissolution and transformation of existing pyrite. Haematite is also present filling fractures that crosscut the unit.

XRD analyses performed on the clay fraction of pelitic levels of both members indicate it is composed of mica (77 to 95%) and chlorite (4 to 23%), with subordinate quartz and plagioclase (Table 1). However, lesser amounts of interstratified Chl/Vrm and Ilt/Chl, kaolinite, and vermiculite were identified in some samples. Particularly, the two samples (PS1, PS2; see Table 1) collected in the Peña Negra locality have subordinate smectite (2 to 10%), whereas the sample collected immediately below the unconformity that separates the Carboniferous from the Volcancito Formation is composed of mica (77%), kaolinite (21%), and smectite (2%). $KI_{(CIS)}$ values in the Río Volcancito section range from 0.33 to 0.39 Δº2θ (n=15), indicating low-anchizone metamorphism. White mica *b* parameter ranges between 9.011 and 9.026Å (n: 4; s: 0.006).

4.1.3.2. Bordo Atravesado Formation

The first record of volcanism in the Ordovician Famatina belt is represented by silicified tuffs that appear in the Bordo Atravesado Formation. This unit consists of finely laminated mudstones to siltstones, interbedded with massive fine-grained silicified sandstones commonly showing parallel to hummocky cross-stratification (Zimmerman and Esteban, 2002; Astini, 2003; Albanesi *et al*., 2005). Silicified episodic tuffs levels have thicknesses between 5 and 35 cm and commonly develop internal layering and syn-sedimentary deformation, indicating abrupt deposition. Microscopically, they constitute homogeneous masses of micro- to cryptocrystalline quartz (chert) locally intergrown with fine-grained white mica and dispersed pyrite cubes. The mud-siltstone levels present clear parallel granulometric-compositional lamination and consist predominantly of very small quartz crystals (up to 0.04 mm), mica, chlorite, organic matter, and opaque mineral aggregates (up to 3 mm).

The sandstones are dominated by quartz grains, mudstone, siltstone, and sandy lithoclasts, calcite, abundant pyrite, zircon (up to 0.1 mm), folded detrital white-mica grains, and scarce feldspar and bioclasts, all in a fine-grained matrix mainly composed of white mica, chlorite (in aggregates of up to 0.2 mm), quartz, and opaque minerals, none of which have any clear orientation. The quartz grains have undulatory extinction, bands, and deformation lamellae, subgrains, and hairy edges in the contact with the clay matrix. In sectors where the matrix is less abundant, contacts range from plane to sutured. Silica overgrowths in optical continuity within quartz grains (probably associated with early cementation) were also observed. Pyrite occurs predominantly as framboidal aggregates and euhedral crystals clearly identifiable in hand sample with edges sometimes altered to chlorite.

The mineralogy of the clay fraction was established in 2 pelitic levels of this unit. The samples are predominantly composed of mica (90-95%), subordinate chlorite (5-10%), and scarce amounts of interstratified chlorite/vermiculite (Chl/Vrm) and vermiculite (Table 1). Chl/Vrm was identified by the (002) reflection at 12Å in the heated diagram, corresponding to a basal spacing of ~24Å, resulting from the sum of the chlorite 14Å and the vermiculite 10Å spacings after collapse due to heating. Vermiculite was identified by decreasing intensity of the reflections at 14Å, 7Å, and 3.58Å in the heated diagram, accompanied by an increase in the intensity of the 10Å reflection. $KI_{(CIS)}$ values for this unit are 0.31 and 0.35 Δº2θ.

4.1.3.3. Famatina Group

4.1.3.3.1. Suri Formation. This unit includes various epiclastic deposits interbedded with volcaniclastic, volcanogenic, and volcanic rocks (Fig. 5c and d; Mángano and Buatois, 1994; Astini, 2003). The pelites from this sequence, mainly located at the base of the unit, range in colour from bluish-grey to black. They have S_0 layering defined by alternating bands with different proportions of phyllosilicates and changes in organic matter contents, and are mainly composed of phyllosilicates, fine-grained quartz, and subordinate opaque minerals. The siltstone levels that alternate with the pelites have sporadic subrounded to subangular quartz grains (up to 0.05 mm), often elongated parallel to S_0 and with undulatory extinction. Some elongated intraclasts were also observed. The sandstones of this unit are

immature and have alternating bands composed of quartz grains and plagioclase, with white mica, chlorite, and biotite, and subordinate opaque minerals, sporadic siltstone intraclasts, and fragmented bioclasts in a silty-clay dominated matrix. Quartz grains have some plane contacts, products of silica overgrowth in optical continuity, but they also show sutured contacts related to pressure-solution processes and, sometimes, subgrains. White mica appears with fringed edges and as thin fibres surrounding larger quartz grains. Biotite frequently has chloritized edges. Detrital chlorite has sticky and, occasionally, fan habits. The anomalous brown interference colour of detrital chlorites indicates a composition with similar proportions of Fe and Mg, corresponding to ferrous clinochlore (Nieto, 1997). Mica grains with intergrown chlorite were also identified. Pyrite is the most abundant opaque mineral, appearing as framboidal aggregates, and irregular to euhedral crystals, but haematite was also identified. The sandstone matrix is composed predominantly of very fine quartz (up to 0.02 mm) and subordinate phyllosilicates. Towards the top of the unit, sandstone levels become thicker and contain abundant volcanic lithics and volcaniclastic grains (varieties of siliceous tuffs and ignimbrites).

The clay mineral fraction (< 2 μm) of the pelites is mainly composed of mica (76-97%), chlorite (3-24%), and quartz, with subordinate plagioclase (Table 1). In the air-dried diagram of some samples, the 14Å reflection is more intense than the 7Å reflection, and it decreases in intensity after heating, together with an increase in intensity of the 10Å, 5Å, and 3.3Å reflections. This behaviour is likely due to the presence of minor amounts of vermiculite, characterized by an intense reflection at 14.2Å that collapsed to 10Å after heating at 500ºC. In another group of samples, the heated diagram shows a reflection around 12Å that probably corresponds to interstratified Chl/Vrm. In one of the samples, an Ilt/Chl mixed-layer (~18%) was also identified. $KI_{(CIS)}$ values in this unit range between 0.41 and 0.59 Δº2θ (n: 15), and the mean white mica *b* parameter is 9.011 (n: 4; s: 0.006).

4.1.3.3.2. Molles Formation. A detailed sedimentological-stratigraphic analysis of the Molles Formation was carried out by Astini and Benedetto (1996), Astini (1998, 2003), and Dávila (2003). The sequence (~500 m in thickness) has volcanic levels alternating with a clastic succession represented by sandstone layers up to 0.2 m thick. Among the volcanic components, Astini (1998) mentioned subvolcanic intrusives with columnar jointing, volcaniclastic deposits, ignimbritic bodies, siliceous tuffs, and accretionary lapilly levels. Muddy interstratified layers are scarce, with local heterolithic lenticular facies where pelites were intensely bioturbated (Dávila, 2003). In pelitic levels, a fracture pencil cleavage S_1 developed subperpendicular to the S_0. The coarser clastic levels (Fig. 5e and f) have abundant rounded or embayed quartz grains, mostly with straight extinction, and abundant grains of potassium feldspar, with a smaller amount of plagioclase, volcanic lithic fragments with porphyritic texture, rhyolitic glass fragments with flux textures (probably ignimbrites), massive to microcrystalline vitreous aggregates, fragmented bioclasts and, less frequently, abundant microcrystalline glauconitic grains. Volcanic glass grains commonly have edges completely transformed to microcrystalline quartz and are covered by a thin layer of clay minerals with high birefringence. Pores are filled with carbonate cement and chlorite aggregates. Detrital grains usually present abundant plane and concave-convex contacts as a result of pressure-solution processes. Between these contacts are found relicts of thin layers of clays covering the detrital grains. Quartz overgrowths in optical continuity with detrital grains were only observed in some levels.

The clay mineralogy of the scarce pelitic layers cropping out in the Molles River locality consists of illite (89-92%), chlorite (8-11%) and quartz (Table 1). In the Cachiyuyo River section, two samples corresponding to layers located a few metres below the discordance that separates the Molles Formation from the overlying Cerro Morado Group mainly comprise interstratified illite/smectite (Ilt/Sme;with 95% illitic layers) and subordinate quartz. In this sequence, $KI_{(CIS)}$ values range from 0.46 to 1.32 Δº2θ (n: 5), corresponding to the early to late diagenetic zones.

4.1.3.4. Cerro Morado Group

4.1.3.4.1. La Escondida Formation. The Cerro Morado Group is separated from the Famatina Group by an angular discordance. It begins with the volcanic-volcaniclastic sequence of El Portillo Formation and continues with the deposition of La

Escondida Formation, which contains some pelitic levels. Most of the psamitic and micro-conglomeratic levels of this sequence are partially silicified. Astini and Dávila (2002) interpreted both the vitreous tuffs and the accretionary lapilly occurring within these levels as falling deposits associated with violent eruptions, linked to subaerial explosions of phreatomagmatic origin, often associated with acid volcanism. Microscopic features evidence viscose fluxes with plastic deformation that contribute to the elimination of porosity.

One of the analysed pelitic levels is located at around 10 m from the base of the unit, whereas the remaining two are in the middle part of the sequence and correspond to yellowish-green bioturbated marine pelites interbedded with yellow sandstone and limestone levels with high brachiopod contents. The pelitic sample at the bottom of the sequence shows a clay-mineral fraction mainly composed of interstratified Ilt/Sme (90-95% illitic layers) with traces of vermiculite. The two remaining samples contain interstratified I/S, similar to that from the previous sample, and also show traces of kaolinite, vermiculite, and chlorite. In all three samples, subordinate quartz and potassium feldspar were also identified (Table 1). $KI_{(CIS)}$ values range from 0.50 to 0.69 $\Delta º2\theta$ (n: 3).

4.1.4. La Aguadita Formation (Upper Ordovician)

This unit can be divided into two informal members, the lower mainly composed of metarkoses (150 m thick) and the upper consisting of alternating metapelite and thin metasandstone levels (Fig. 6). S_0 can be recognized and is overprinted by a subparallel to oblique secondary S_1 foliation (350°N/63°E). In the upper member, foliation is microscopically defined by the orientation of the (001) planes of neoformed and transformed phyllosilicates and the direction of the long axis of the quartz and feldspar grains. The S_1 plane is interpreted as the product of the mechanical rotation and deformation of detrital minerals by pressure-solution and recrystallisation processes, which generate a fine-grained matrix parallel to the foliation (P domains; Knipe, 1981) and modified detrital grains parallel to the S_1 foliation that is not as strong (Q domains). Metapelites are very fine-grained with centimetric bedding generated by alternating clay and silt-clay layers, which reflect the sedimentary S_0. The neoformed phyllosilicates are arranged around the larger grains so that their (001) planes are orientated defining metamorphic S_1 foliation oblique to subparallel to S_0. Back-scattered electron images indicate that pelites from La Aguadita Formation are composed of quartz, K-white mica, chlorite, K-

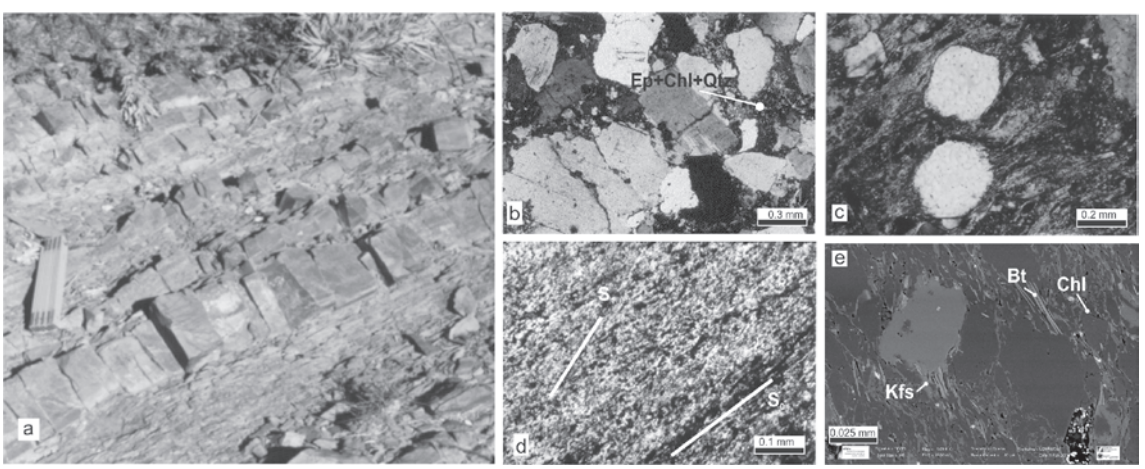

FIG. 6. La Aguadita Formation. **a.** Outcrop view of the Upper Member with alternance of metasandstones and shales; **b.** Metaarkose from the Lower Member; **c.** Metasandstone showing quartz-feldspathic grains surrounded by a quartz-mica matrix defining a blastopsamitic to granolepodoblastic S_1 foliation. These crystals have clear grain boundaries parallel to the S_1 foliation, whereas the perpendicular edges are diffuse and develop pressure shadows with beards of mica, quartz, and chlorite, typical of dissolution-recrystallization processes. Potassium feldspar is usually altered to fine-grained white mica; **d.** Metapelite with granulometric-compositional layering belonging to the S_0 foliation and the orientation of neoformed phyllosilicates defining the S_1 secondary foliation; **e.** Typical representative texture of metasandstone at backscattered electron scale.

feldspar, and scarce epidote, which together define a soft cleavage (cf. Passchier and Trouw, 1998). In addition, blastic biotite up to 2 μm in thickness and mainly associated with pressure shadows was identified in two of the samples. K-white mica and K-feldspar constitute large domains (>50 μm) mostly orientated according to the well-developed slaty cleavage; they present diffuse contacts indicative of their concomitant development.

Metagreywackes have a blastopsamitic to granolepidoblastic texture producing rough cleavage. The primary compositional layering (S_0) is evidenced by alternating millimetric bands composed of quartz, potassium feldspar, and plagioclase grains surrounded by an epidote-quartz-mica matrix. XRD whole-rock analyses show that metagreywackes from the upper member mainly comprise quartz, chlorite, mica, epidote, plagioclase, potassium feldspar, and smectite (Table 1).

In the lower member, metarkoses have a clastic to blastopsamitic texture with millimetric quartz-feldpar grains surrounded by a scarce matrix, predominantly composed of fine-grained white mica and abundant opaque minerals. XRD analyses performed on representative samples indicate that metarkoses are composed of quartz, chlorite, mica, epidote, potassium feldspar, and plagioclase. In some samples, dioctahedral mica is present in low proportions, and in others it is totally absent.

Epidote blasts (as tabular grains or 1.5 mm aggregates) identified in metarkoses and metasandstones replace detrital plagioclase and are mainly associated with anhedral to radial chlorite, calcite (0.15 mm.), and pyrite; they have been interpreted as the product of pervasive hydrothermal propylitic alteration (Collo *et al*., 2005).

The clay fraction from La Aguadita Formation metapelites mainly consists of mica (61-94%) with subordinate chlorite (4-9%). All these rocks have minor amounts of smectite (2-6%) and associated vermiculite, kaolinite, and interstratified Ilt/Sme (R0), Ilt/Chl, and Chl/Vrm (Table 1). Given the presence of smectite in all the analysed samples, $KI_{(CIS)}$ values were measured both in air-dried and glycolated aggregates with similar results. $KI_{(CIS)}$ values from this unit range between 0.40 and 0.26°Δ2θ (n: 6), indicating low to high anchizone conditions (Table 1). Moreover, SEM analyses identified blastic biotite in two samples, demonstrating that this unit attained green-schist facies metamorphism (~400ºC). Consequently, smectite vermiculite, kaolinite, as well as interstratified Ilt/Sme (R0), Ilt/Chl, and Chl/Vrm phases were interpreted as retrograde diagenesis products (Collo *et al*., 2005). No relationship was identified between the KI values and the stratigraphic position of the samples in this section.

The white mica *b* parameter measured for fine-grained rocks from this unit has a mean value of 9.024 (n: 4; s: 0.004, Table 1) corresponding to the intermediate-pressure facies series of Guidotti and Sassi (1986). Therefore, according to the temperature deduced from mineralogy and KI values, a medium palaeogeothermal gradient (~25°C/km) can be inferred, similar to those obtained for the oldest Negro Peinado Formation.

4.2. Chemical composition of phyllosilicates from Negro Peinado, Achavil and La Aguadita Formations

4.2.1. Pampean synorogenic suites: The Negro Peinado and Achavil formations

Neoformed white micas within the Negro Peinado Formation show Fe+Mg contents of 0.12-0.59 apfu, silica contents of 3.06-3.39 apfu, and interlayer charges of 0.82-1.03 apfu. In samples containing blastic biotite, dioctahedral mica compositions are close to the muscovite end member (Appendix A). Fe^{3+}/Fe_{Tot} (XFe^{3+})=0.75 was used in the calculations of structural formulae given the presence of haematite associated with the mica blastesis (Guidotti *et al*., 1994). Although moderate dispersion could be observed in the white mica composition from this unit, analyses carried out in individual samples show little internal variations (Fig. 7), which is in accordance with advanced compositional homogenization. It is worth emphasizing that, with the exception of a few grains, these micas do not show significant illitic substitution ($SiAl_{-1}\square K_{-1}$).

In the Achavil Formation, XFe^{3+}=0.50 was employed in the calculations of dioctahedral mica structural formulae due to the presence of pyrite and ilmenite in these samples. White micas from this unit show a greater dispersion in Fe+Mg contents (0.11-0.70 apfu), and similar silica contents (3.05-3.43 apfu) and interlayer charge (0.82-1.02 apfu) than the ones from the Negro Peinado For-

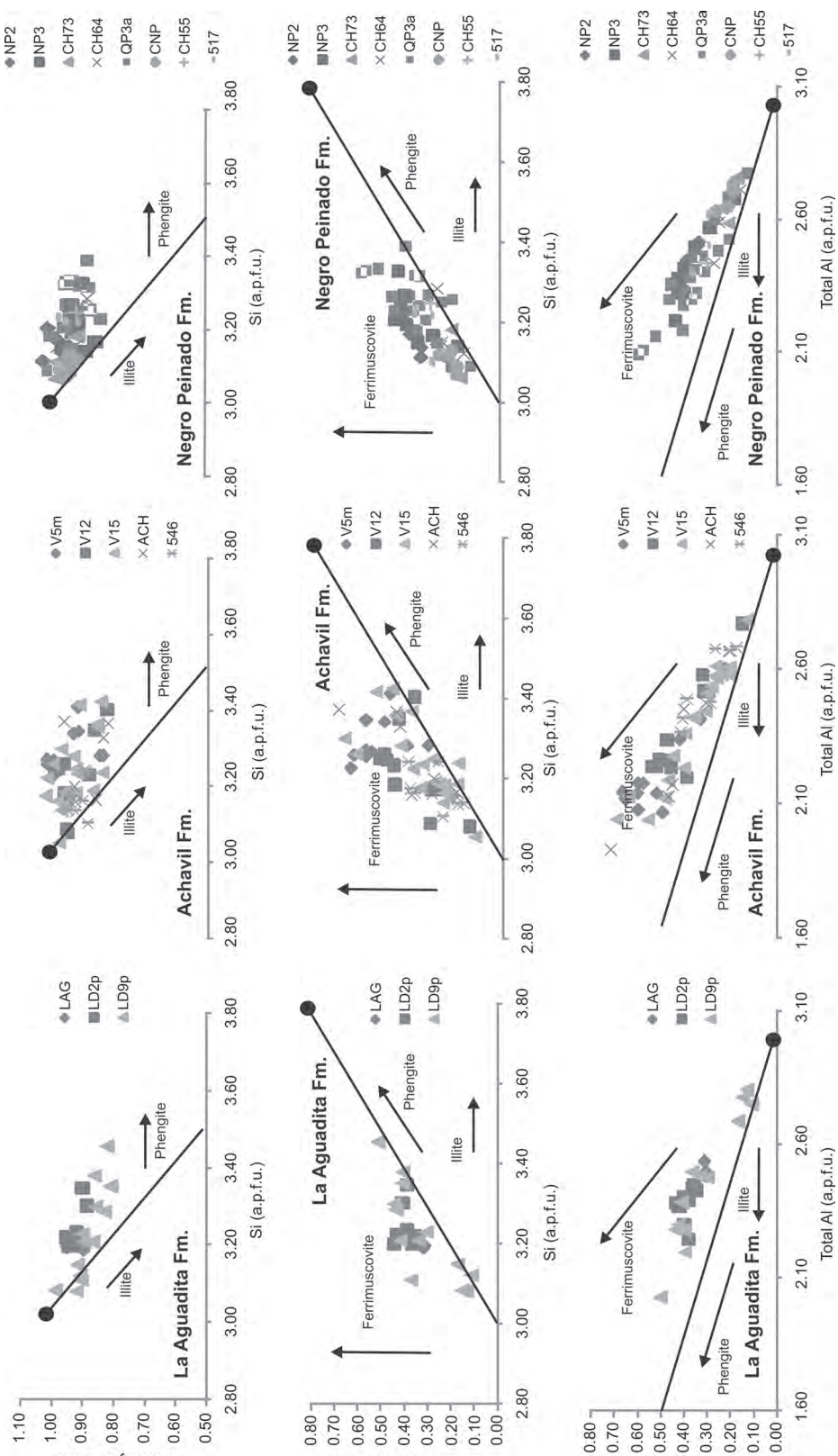

FIG. 7. Diagrams showing chemical compositions of dioctahedral phyllosilicates in Negro Peinado, Achavil, and La Aguadita formations; solid circles and lines indicate theoretical muscovite compositions and arrows represent different exchange vectors.

mation (Appendix A; Fig. 7). Moreover, micas from this unit show greater internal variation in individual samples than the ones from the Negro Peinado Formation, indicating a lack of chemical equilibrium between neoformed phases.

Dioctahedral micas from both units show clear phengitic substitution and a few analyses depict scarce paragonitic substitution (Na^+ contents generally up to 0.11 apfu in the Negro Peinado Formation and up to 0.17 apfu in the Achavil Formation). Na^+ contents reaching 0.78 apfu in one sample from the last unit (see ACH in Appendix A) may be attributable to intermediate meta-stable Na-K micas or to paragonite and muscovite intergrowths at a very small scale (Livi *et al*., 2008). Some ferrimuscovitic substitution can also be inferred for both units considering the difference between (Si-3)-Mg and Fe contents as reflecting the presence of Fe^{3+}.

Chlorite from the Negro Peinado Formation presents Fe/Fe+Mg ratios between 0.43 and 0.63, corresponding to ferrous clinochlore to magnesian chamosite (Appendix B). Fe and Mg show an inverse tendency compatible with the FM substitution ($FeMg_{-1}$, Fig. 8; Laird, 1988). $Al^{IV}(Fe, Mg)_{-1}Si_{-1}$ substitution seems to be somewhat unimportant, as indicated by the total Al values (Fig. 8). The same tendencies were observed for the Achavil Formation, although in this unit chlorite has a wider compositional range. In fact, chlorites from the three analysed samples outline three different groups in the Fe *versus* Mg diagram. Chlorites from the Achavil Formation show Fe/Fe+Mg ratios of 0.36 to 0.65 (Clinochlore to magnesic chamosite), with a narrow range (0.45-0.49) in the 546 sample. Chlorite from both units plots close to the full octahedral occupancy line in the diagram proposed by Hillier and Velde (1991), what is characteristic of metamorphic chlorites (Fig. 8), although some grains with higher Si contents in the Achavil Formation are in accordance with its lower grade. The lower dispersion in chlorite compositions in the Negro Peinado Formation is consistent with the narrower range in Fe/Fe+Mg ratios depicted by white micas in this unit.

In the Negro Peinado Formation, subordinate di-trioctahedral substitution was also identified (Fig. 8). These grains are characterized by their lower octahedral cation sums and Fe+Mg contents and higher Si and Al contents than other chlorites.

4.2.2. Ocloyic synorogenic suite: La Aguadita Formation

In this unit, XFe^{3+}=0.75 was used in the calculations of dioctahedral mica formulae given the presence of haematite associated with the mica blastesis. White mica has Fe+Mg contents of 0.11-0.51 apfu, silica contents of 3.08-3.46 apfu, and interlayer cation contents of 0.80-0.98 apfu (Appendix A; Fig. 7). A direct correlation between Si and Fe+Mg contents is consistent with phengitic substitution. Paragonitic substitution is very low in general, but one grain with Na contents up to 0.12 apfu is also present. Some ferrimuscovitic substitution can also be inferred based on the difference between (Si-3)-Mg and Fe.

Chlorites from La Aguadita Formation have Fe/Fe+Mg ratios of 0.51-0.65 (Appendix B; Fig. 8), corresponding to magnesian chamosite. Most of the analyses plot near the fully octahedral occupancy line consistent with metamorphic chlorites. Some grains depicting slightly higher Si contents could correspond to diagenetic chlorite (Hillier and Velde, 1991).

4.3. Phengite geobarometry

Since the Si content of white mica is affected by phengitic and illitic substitutions, the illitic component should be taken into account for a correct use of the phengite geobarometer (Agard *et al.,* 2001; Abad *et al*., 2006). Therefore, phengites from the three analysed units that evidenced illitic substitution (interlayer charge <0.85 and (Si-3) higher than Mg+Fe content) were excluded from the geobarometric calculation. Omitting grains with illitic substitution, maximum Si contents in individual samples ranges from 3.12 to 3.39 apfu in the Negro Peinado Formation and from 3.20 to 3.42 apfu in the Achavil Formation (Appendix A). Pelites from the two units do not contain the limiting paragenesis Ms-KFsp-Qz-Phl, and consequently the estimated pressures should be considered minimum values (see Massone and Schreyer, 1987). Using the recalculated Si isopleths grid published by Massone and Szpurka (1997), and considering the estimated maximum temperatures according to $KI_{(CIS)}$ and mineralogy , values between ~1 and ~4.5 kbar can be estimated for the Negro Peinado Formation and between ~1 and 4 kbar for the Achavil Formation. In turn, two

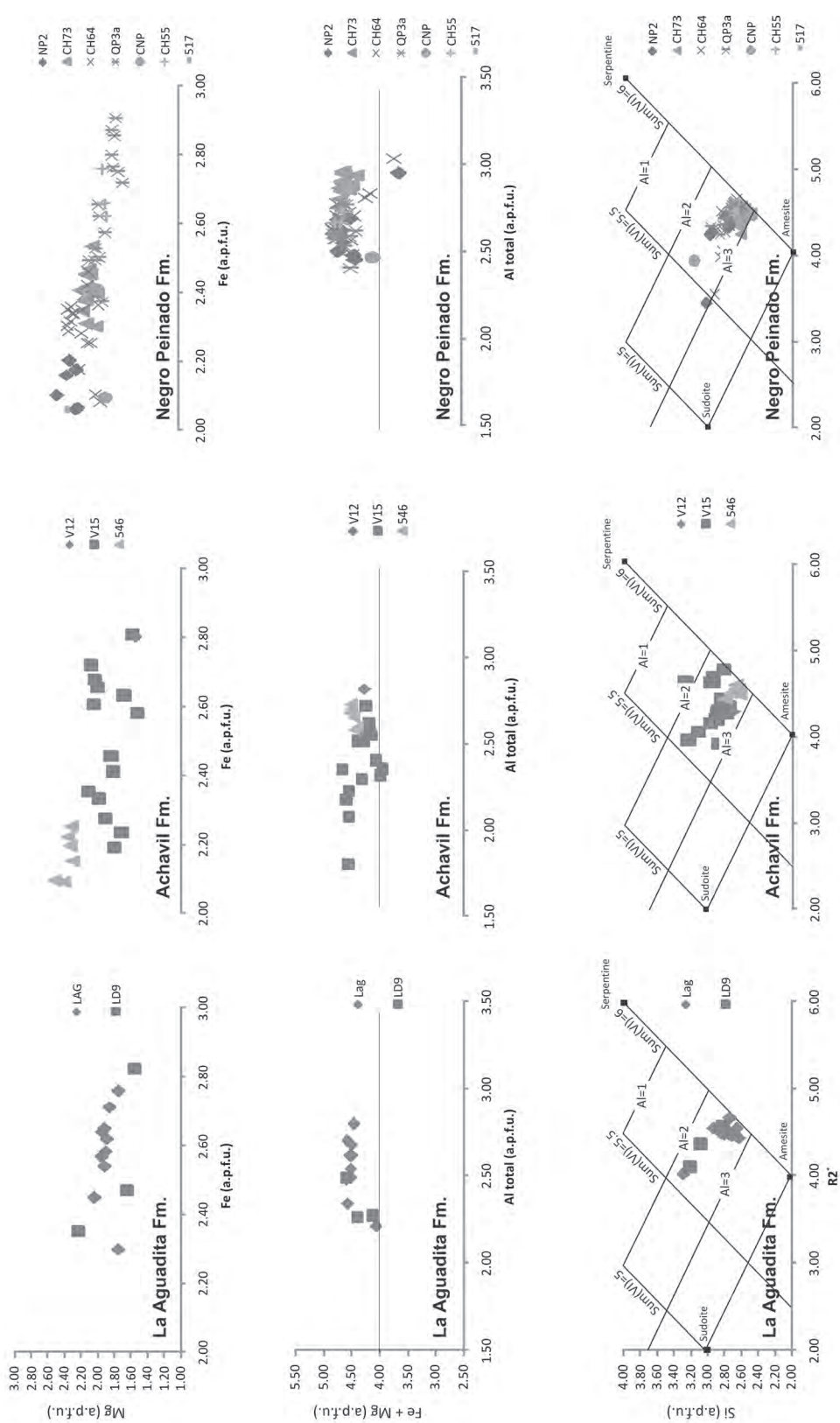

FIG. 8. Chemical composition diagrams of chlorites from Negro Peinado, Achavil, and La Aguadita formations.

samples from La Aguadita Formation presenting the limiting paragenesis (LD2p and LD9p) show silica contents of up to 3.23 and 3.35 apfu, respectively, suggesting maximum pressure conditions of around ~2.5 and ~5 Kbar.

5. Discussion

5.1. Characterization of the metamorphic-deformational episodes affecting the low-grade units

5.1.1. The Middle-Upper Cambrian Negro Peinado Formation

The recrystallization and pressure-solution processes identified in the rocks of the Negro Peinado Formation, the development of S_1 foliation in phyllite and meta-sandstone levels, the presence of final members of the di- and tri-octahedral reaction series (namely phengite and chlorite, respectively), as well as the local biotite blastesis are clear indicators of the succession having been affected by low-grade metamorphism. These results, along with measured crystallographic parameters, point to a metamorphic-deformational event, $M1_{NP}$-$D1_{NP}$, associated with intense intrafoliar folding $P1_{NP}$ in greenschist facies, ranging from high anchizone to epizone to the biotite zone (~290-400°C), and under intermediate pressure (Fig. 9). No metamorphic trend was observed in the sequence.

5.1.2. The Middle-Upper Cambrian Achavil Formation

The Achavil Formation also shows clear petrographic evidence of metamorphic transformations such as reorientation of detrital grains, intracrystalline deformation, pressure-solution, and mineral recrystallization, although in most locations it preserves its sedimentary attributes. High anchizonal $KI_{(CIS)}$ values from this unit are consistent with the clay mineral association recognized in metapelites,

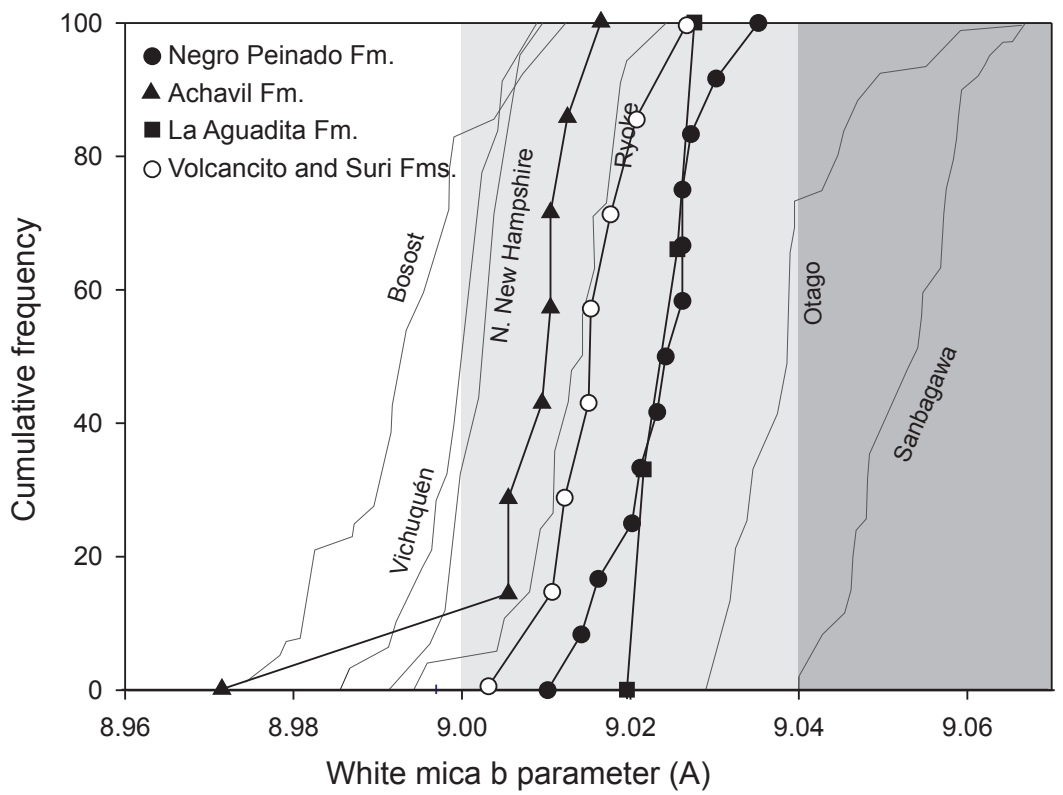

FIG. 9. Cumulative frequency *versus b*-parameter values. As reference low-pressure (white), intermediate-pressure (light grey), and high-pressure (dark grey) fields from Guidotti and Sassi (1986) are shown, and curves from other well-characterized low-grade metamorphic terranes are added (cf. Sassi and Scolari, 1974).

and define a main metamorphic event $M1_{ACH}$ with estimated temperatures reaching ~290°C and intermediate- to low-pressure conditions. Although textural relations between $M1_{ACH}$ and the deformational episodes $P1_{ACH}$ and $P2_{ACH}$ could not be clearly established, the oblique cleavage probably developed in association with the second folding episode.

5.1.3. The Cambro-Ordovician volcaniclastic units

For the Cambro-Ordovician volcaniclastic sequence overlying the Achavil Formation, metamorphic conditions from anchizone to late diagenesis are interpreted on the basis of $KI_{(CIS)}$ values (Fig. 10), that show a clear tendency to more intensive post-depositional changes in the more deeply buried rocks. A clear prograde trend can also be established considering the distribution of the neoformed clay minerals throughout the sequence, with illite and chlorite as the main phyllosilicates in the oldest units and almost solely Ilt/Sme (R3) in the youngest. This decrease in grade from the Volcancito Formation to La Escondida Formation follows a trend consistent with burial metamorphism.

Changes in clay mineral assemblages of pelitic levels within each unit, such as the total absence of chlorite in the upper levels of the Molles Formation and in pelites from La Escondida Formation (Cerro Morado Group), contrasting with more than 10% in other levels, could be associated to changes in the type of source material in the basin. The predominance of mica in these units is probably due to an increase in the supply of rhyolitic components. This contribution is clear in the coarser-grained rocks, as mentioned by Astini and Dávila (2002). From a textural point of view, it can be seen that the processes of mineral recrystallization are more intense in the Volcancito Formation rocks, whereas in younger successions they are rare or absent. At the same time, a decrease in intracrystalline deformation as well as in pressure-solution processes is evident towards the top of the sedimentary column. The relative abundance of serrated contacts in rocks of the older units with respect to the younger ones evidences the differential strength of these processes.

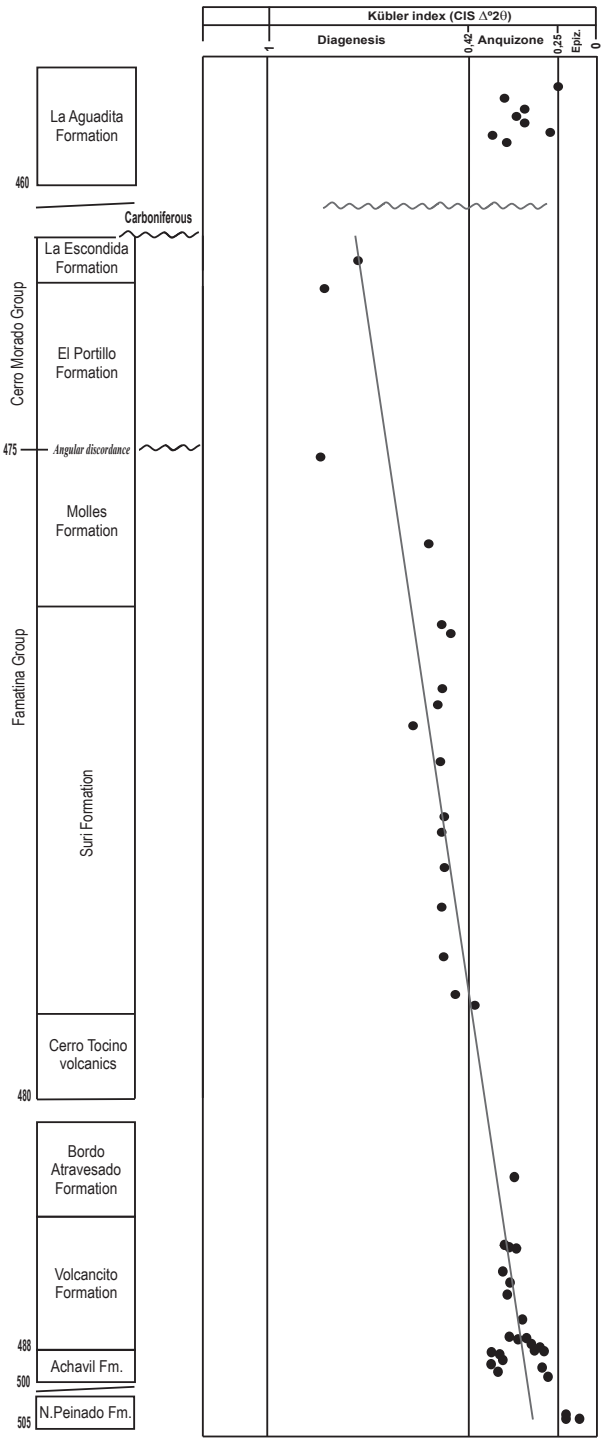

FIG. 10. Kübler index value distribution along the sequences. The decrease in metamorphic grade towards the younger sequences can be clearly observed, as well as the visible break between the Ordovician volcaniclastic units and the middle Ordovician La Aguadita formation.

Considering the Cambro-Ordovician succession cropping out in the central-western sheets (from the Volcancito to La Escondida formations), it can be observed that neoformed phyllosilicates are predominantly orientated parallel to S_0. The marked parallelism between the sedimentary S_0 and the secondary cleavage defines a compaction fabric (compaction cleavage) in most of the units, suggesting that the post-depositional changes would have been associated with the sequence burial, suggesting that the main burial episode would not have been linked to a major deformational episode. The disposition of neoformed minerals alongside the sedimentary layering established for the fine-grained rocks indicates that the maximum P-T conditions, and thus the diagenetic-metamorphic grade reached by the sequence, were controlled by basin subsidence processes.

The white mica *b* parameter measured in Volcancito and Suri formations suggests conditions close to the boundary between intermediate and intermediate-low pressure facies series (Guidotti and Sassi, 1986). The cumulative frequency curve for the white mica *b* parameter of all the rocks corresponding to this structutal sheet resembles the curve for the eastern sector of the orogenic belt of Royke (Fig. 9), assigned to low to intermediate-low pressure facies series, with an average *b* parameter of *b* 9.015Å (Sassi and Scolari, 1974).

Based on $KI_{(CIS)}$ values, temperatures between ~ 240-255°C can be established for the bottom of the Cambro-Ordovician column (about 4,000 m preserved), with temperatures between ~125-145ºC estimated for the upper levels. This increase in temperature with depth (~130ºC in 4,000 m) with a relatively constant slope (see Fig. 9), is consistent with a gradient of approximately 33ºC/km, similar to that suggested from the *b* parameter.

Colour alteration indices (CAI) for conodonts recovered from the Suri Formation (2-3; Albanesi and Astini, 2000) are consistent with the temperatures estimated for this unit (~165-200°C). CAI values between 2 and 5 obtained for the Lower Member of the Volcancito Formation (Albanesi *et al.*, 1999) suggest a not well constrained temperature range (60-140ºC and 300-480ºC for minimum and maximum temperatures, respectively) in comparison to that set by the petrographic and mineralogical analysis (~210-240°C). Moreover, textural features (*e.g.*, sutured contacts and undulatory extinction in quartz grains, stylolites), indicates that the sequence was affected by pressure-solution processes and intracrystalline deformation consistent with the conditions established through $KI_{(CIS)}$ and clay mineralogy.

5.1.3.1. Significance of Chl/Vrm through the Cambro-Ordovician succession

Subordinate clay-mineral phases such as Chl/Vrm, kaolinite, smectite, vermiculite, and Ilt/Chl appear throughout the Cambro-Ordovician sequence. Interstratified Chl/Vrm present in some samples could correspond to a metaestable phase from which chlorite formed, being part of the prograde reaction series corrensite→corrensite-chlorite→chlorite. The presence of intermediate phases belonging to this series, in which the vermiculite would be generated by detrital biotite alteration (Bozkaya and Yalçin, 2004), is consistent with late diagenetic conditions (Jiang and Peacor, 1994; Merriman and Peacor, 1999). However, some of the samples containing interstratified Chl/Vrm show $KI_{(CIS)}$ values corresponding to high-anchizone conditions (*e.g.*, Achavil Formation), under which Chl/Vrm is generally not stable, and it seems more likely they are the product of retrograde reactions. It should be noted that some millimetric veins of chlorite+opaque minerals were identified in the metapelites. Within this setting, vermiculite and Chl/Vrm could be the product of chlorite alteration under oxidizing conditions (Gaudin *et al.*, 2005), as evidenced in the coarse-grained rocks, likely associated with localized interaction with post-metamorphic fluids. Moreover, kaolinite and smectite would be the product of local alteration (hydrolysis) of feldspar and illite in the rocks during or after exhumation of the sequence. This seems to be the case for sample AC-V, taken near the top of the Volcancito Formation immediately below the discordance with the Carboniferous, in which kaolinite (21%) probably results from the predominant transformation of feldspars interacting with meteoric water following the uplift of the unit.

5.1.4. The youngest La Aguadita Formation

The upward transition from anchizonal to diagenetic grade is clear in the Cambro-Ordovician sequence from the central-western sheets within the Famatina belt. However, the eastern and youngest La Aguadita

Formation (deposition after *ca*. 452 Ma, Astini *et al*., 2003) depicts a sharp increase in metamorphic conditions in comparison with the upper levels croping out in the central-western sheets (Fig. 10). The existence of a tectonic fabric (S_1), oblique to S_0, shows that metamorphic processes here were concomitant with a deformational episode during which the detrital and neoformed grains were orientated perpendicular to the main strain; suggesting an intense metamorphic-deformational ($M1_{LA}$-$D1_{LA}$) event (Collo *et al*., 2005). This main metamorphic-deformational episode attained anchizone to greenschist facies (temperatures reaching ~400°C) and intermediate-pressure facies series (see Fig. 9).

A post-$M1_{LA}$ propylitic hydrothermal event can be inferred for this unit taking into account the compositional variation observed between coarse-grained rocks (with epidote, chlorite, calcite, and pyrite) and metapelites. In several systems with propylitc alterations, the first appearance of epidote has been recorded over the 200°C isotherm (Bird and Spieler, 2004). Moreover, the presence of smectite and interstratified Ilt/Sme (R0) in the <2μm fraction of La Aguadita Formation metapelites is incompatible with both the medium-anchizonal degree and the development of metamorphic foliation. These phases could be the result of the interaction of fluids with the rocks during the cooling of the hydrothermal system that generated the propylitic association in coarse-grained rocks, or to the influence of meteoric water after exhumation (Collo *et al.*, 2005). Both processes can be regarded as retrograde diagenetic events (Nieto and Peacor, 1993; Nieto *et al.*, 1994; Merriman and Peacor, 1999) as this term, according to its most recent definition (Nieto *et al.*, 2005), covers all very low-temperature processes occurring during the ascent of the rocks to the surface after the metamorphic peak, including hydrothermal alterations. It is clear that the genesis of these retrograde phyllosilicates in La Aguadita Formation metapelites took place after the prograde mica and chlorite formation (270-330ºC).

5.2. Mica chemical compositions and metamorphic conditions

Although textural and compositional changes taking place within diagenetic to low epizone conditions are gradual and difficult to quantify, a trend towards chemical and textural homogenization, including an increase in grain size of phyllosilicates, is clear in rocks above the epizone (Nieto and Abad, 2007). This trend can be clearly observed in both the Famatinian Cambrian Negro Peinado and Achavil formations, but also in the Upper Ordovician La Aguadita Formation, cropping out in the eastern belt and affected by the strongest metamorphic conditions. The Negro Peinado Formation shows compositional homogeneity in dioctahedral micas consistent with epizonal metamorphism (Abad *et al.*, 2006). The Achavil Formation has compositional features, especially in dioctahedral micas, indicating a lower metamorphic grade, as was previously established through the Kübler index. In spite of its younger age, La Aguadita Formation reveals an intermediate behaviour between the Negro Peinado and Achavil Formations in terms of phyllosilicate evolution.

The large dispersion in the pressures estimated through the phengite geobarometer for the Achavil, Negro Peinado and La Aguadita formations could indicate continuous crystallization of micas over the entire decompression path (Abad *et al.*, 2003). Moreover, a careful treatment of this geobarometer is required given the lack of chemical and thermodynamic equilibrium even at individual sample scale in anchizonal to low-grade metamorphic rocks, frequently resulting in the coexistence of metastable phases. Moreover, it is worth to emphasize that modifications of ~50°C in temperature estimations change substantially the obtained pressure values.

5.3. Regional implications of the low-grade metamorphism in the Famatina belt

Although the post-depositional history in sedimentary basins associated with arc and back-arc settings is frequently complex, two contrasting situations can be considered depending predominantly on the relationship between heat flow and deformation. In cases where gradients are high and deformation is not very strong, a direct relationship between the increase in metamorphic grade and the age of the affected sequences is expected, what is known as the burial metamorphic pattern. On the other hand, when tectonic stress predominates, the above-mentioned relationship does not occur, and then the metamorphic grade does not necessarily increase from younger to older units. The post-

depositional evolution of the Cambro-Ordovician Famatinian units cannot be fully explained by only one of these extreme models.

The Negro Peinado Formation presents a tight isoclinal folding synchronous with metamorphism (phyllosilicates oriented non-parallel to S_0) likely associated with contraction at a convergent plate margin (Merriman and Peacor, 1999). This unit is intruded in several localities by Early-Middle Ordovician granitoids (*ca.* 484-463 Ma, Pankhurst *et al.*, 2000; Dahlquist *et al.*, 2008) associated with crustal recycling, that developed contact metamorphic aureoles whose textures indicate that the intrusion was coeval with the folding affecting Negro Peinado rocks. Thus, the age of the main metamorphic episode affecting these rocks could be constrained between *ca.* 485-460 Ma. The few K-Ar ages available for the Negro Peinado Formation are roughly consistent with an Ordovician syntectonic metamorphic event (*ca.* 463-457 Ma, Collo *et al.*, 2008), and compatible with the crustal thickening events proposed for the region immediately after granitoids intrusions (Dalhquist *et al.*, 2008).

The post-depositional evolution of the Middle-Upper Cambrian Achavil Formation is more difficult to unravel. Two possible interpretations could be made for the metamorphism affecting the Achavil Formation: **1.** it could have taken place prior to the deposition of the Volcancito Formation (*ca.* 490 Ma), and contemporary to one of the deformational phases affecting the unit; or alternatively; **2.** maximum burial conditions could have been reached after the deposition of the entire volcaniclastic column (*ca*. 460 Ma). The first hypothesis is supported by the development of the main secondary microscopic foliation oblique to the sedimentary layering; the second one is based on the fact that no significant break is recorded between maximum metamorphic conditions and pressure facies series between the Achavil and Volcancito formations, in spite of the existing discordance between them (~490; Collo and Astini, 2008). In this context, the oblique metamorphic foliation in the Achavil Formation could be interpreted as developed before the deposition of the Volcancito Formation (*ca*. 490 Ma), whereas maximum burial conditions, recorded by phengitic substitution in white micas, would be reached after the deposition of the complete Cambro-Ordovician succession (after *ca*. 460 Ma). A coeval metamorphism and a prograde transition between the Achavil and the Negro Peinado formations previous to *ca*. 490 Ma is difficult to conciliate with ages of the granitoids and the textural relations between them and the last unit. Similar orientations between folding in Negro Peinado Formation and P_2 folding in Achavil Formation are not enough to argue an equivalent folding episode as, since the Ordovician, compressive events in the region have involved predominantly W-E shortening. Evidences of earlier deformational phases in Negro Peinado Formation could have been obliterated by the following and main tectonic episode. On the other side, for the younger units we can clearly establish a correlation between sedimentary age and metamorphic grade from the Volcancito Formation to the Cerro Morado Group throughout the sequence in the central-western sheets (Fig. 10). This relationship occurs despite the existing discordances between the Famatina and Cerro Morado groups (~470 Ma; Dávila *et al*., 2003) as there are no breaks in $KI_{(CIS)}$ trends between these units. Moreover, other burial indicators, such as the cleavage development and textural features mentioned above, also point to a lack of any break in metamorphic grade in these Cambro-Ordovician sequences. This relative continuity indicates that for these units the burial was not episodic, with significant basin inversion events and discrete metamorphic cycles. On the contrary, it could be inferred that it took place in a single event, affecting the whole Cambro-Ordovician volcaniclastic sequence, and post-dating the afore-mentioned discordance. Overall, the increase in metamorphic grade, from deep diagenesis to high anchizone, from younger to older units, is consistent with a burial metamorphic pattern (cf. Merriman and Peacor, 1999). In such a pattern, the diagenetic-metamorphic grade reached by the sequence is controlled by basin subsidence regimes, probably over a thin and hot lithosphere, typical of arc regions within subduction zones (Hyndman *et al*., 2005; Currie and Hyndman, 2006), as is supported by the estimated P/T conditions for central-western sheets. However, a marked break in this burial metamorphic pattern occurs between the younger units of central-western sheets and the upper Ordovician levels of La Aguadita Formation, as the last one depicts strongest metamorphic-deformation conditions than the older Ordovician sequences cropping out to the west (Fig. 10).

The burial metamorphic pattern, as well as the intermediate- to low-pressure conditions inferred

for the Cambrian-Ordovician volcaniclastic successions within the Famatina belt, are broadly consistent with the proposed back-arc extension between *ca*. 480-460 Ma in this region. Moreover, a subsequent crustal thickening and orogenic exhumation at a hinterland position and later local deposition and tectonic burial in a retro-foreland basin to the east are supported by the data. The differential metamorphism of La Aguadita Formation is likely the result of orogenic shortening and coeval tectonic stacking associated with the progressive advancement of the fold-thrust belt from the west towards the foreland after *ca*. 452 Ma. The preservation of the burial metamorphic pattern to the west could be accounted by considering a dominant tectonic inversion within the arc region during the final stages of the Ocloyic orogeny (Fig. 2; 460-435 Ma stage). Differences between intermediate-pressure metamorphism in La Aguadita Formation and low-pressure metamorphism associated to extension described for the other Ordovician units croping out to the east and north (Steenken *et al.*, 2006; Delpino *et al.*, 2007; Fernández *et al.*, 2008; Verdecchia, 2009) could be attributed to their diachronic development. The characteristics of the tectono-metamorphic event that affected La Aguadita Formation indicate a compressive regime that is compatible with the termination of the subduction and with the beginning of the terrane collision and lithosphere cooling and thickening (cf. Hyndman *et al.*, 2005). Further thermobarometric and geochronologic analyses seem to be necessary to better understand the post-depositional evolution of the Negro Peinado and Achavil formations.

Acknowledgements

We are grateful to the Consejo Nacional de Investigaciones Científicas y Técnicas, the Agencia Nacional de Promoción de Ciencia y Tecnología, the Secretaría de Ciencia y Tecnología of the Universidad Nacional de Córdoba and Research Project CGL2007-66744-C02-01 (Spanish Ministry of Science and Technology), which all supported our Research Projects in western Argentina. The stay of G. Collo and M. Do Campo at the University of Granada and the field work of F. Nieto in Argentina were supported by AECI projects A/5120/06 and A/7712/07. We acknowledge Dr. R. Astini for his constructive review of the manuscript, I. Guerra Tschuschke for help with the SEM analyses, which were performed at the Centro de Instrumentación Científica, Universidad de Granada, and J. Santamarina for the measurement of *b* parameter values. C. Laurin helped with the English in the manuscript. The authors also thank thorough reviews by Dr. C. Casquet and an anonymous reviewer and the editorial recommendations that allowed improving this work.

References

Abad, I.; Nieto, F.; Velilla, N.; Mata, P. 2001. The phyllosilicates in diagenetic-metamorphic rocks of the South Portuguese Zone, southwestern Portugal. Canadian Mineralogist 39: 1571-1589.

Abad, I.; Gutiérrez-Alonso, G.; Nieto, F.; Gertner, I.; Becker, A.; Cabero, A. 2003. The structure and the phyllosilicates (chemistry, crystallinity and texture) of Talas Ala-Tau (Tien-Shan, Kyrgyz Republic): comparison with more recent subduction complexes. Tectonophysics 365: 103-127.

Abad, I.; Nieto, F.; Gutiérrez-Alonso, G.; Do Campo, M.; López-Munguira, A.; Velilla, N. 2006. Illitic substitution in micas of very low-grade metamorphic clastic rocks. European Journal of Mineralogy 18: 59-69.

Agard, P.; Vidal, O.; Goffé, B. 2001. Interlayer and Si content of phengite in HP-LT carpholite-bearing metapelites. Journal of Metamorphic Geology 19: 477-493.

Albanesi, G.L.; Astini, R.A. 2000. New conodont fauna from Suri Formation (Early-Middle Ordovician), Famatina System, western Argentina. Ameghiniana 37 (4): 68R.

Albanesi, G.L.; Esteban, S.B.; Barnes, C.R. 1999. Conodontes del intervalo del límite Cámbrico-Ordovícico en la Formación Volcancito, Sistema de Famatina, Argentina. Temas Geológico-Mineros, Instituto Tecnológio Geominero de España 26: 521-526.

Albanesi, G.L.; Esteban, S.B.; Ortega, G.; Hünicken, M.A.; Barnes, C.R. 2005. Bioestratigrafía y ambientes sedimentarios de las Formaciones Volcancito y Bordo Atravesado (Cámbrico Superior-Ordovícico Inferior), Sistema de Famatina, provincia de La Rioja. *In* Geología de la provincia de La Rioja, Precámbrico-Paleozoico Inferior (Dahlquist, J.A.; Baldo, E.G.; Alasino, P.H.; editores). Revista de la Asociación Geológica Argentina, Serie D, Publicación Especial 8: 42-64.

Astini, R.A. 1998. Stratigraphic evidence supporting the rifting, drifting and collision of the Laurentian Precordillera terrane of western Argentina. *In* The Proto-Andean margin of Gondwana (Pankhurst, R.J.; Rapela, C.W.; editors). Geological Society, London, Special Publication 142: 11-33.

Astini, R.A. 2001. Nuia y Girvanella a través de la transición cambro-ordovícica (Formación Volcancito) en el Famatina: significado paleoambiental, paleoclimático y paleogeográfico. Ameghiniana 38: 243-255.

Astini, R.A. 2003. The Ordovician proto Andean basins. *In* Ordovician fossils of Argentina (Benededtto, J.L.; editor). Universidad Nacional de Córdoba: 1-74. Córdoba.

Astini, R.A.; Benedetto, J.L. 1996. Paleoenvironmental features and basin evolution of a complex volcanic-arc region in the Pre-Andean western Gondwana: The Famatina belt. *In* International Symposium on Andean Geodynamics, No. 3, Extended abstracts: 755-758. St. Malo.

Astini, R.A.; Dávila, F.M. 2002. El Grupo Cerro Morado (Ordovícico Medio) en el Famatina (28º-29ºS), Andes Centrales del oeste argentino. Revista Geológica de Chile 29 (2): 241-254.

Astini, R.A.; Dávila, F.M. 2004. Ordovician back arc foreland and Ocloyic thrust belt development on the western Gondwana margin as a response to Precordillera terrane accretion. Tectonics 23: TC4008. DOI:10.1029/2003TC001620

Astini, R.A.; Dávila, F.M.; Rapela C.W.; Pankhurst, R.J.; Fanning, C.M. 2003. Ordovician back-arc clastic wedge in the Famatina Ranges: New ages and implications for reconstruction of the Proto-Andean Gondwana Margin. *In* Ordovician from the Andeds (Albanesi, G.L.; Beresi, M.S.; Peralta, S.H.; editors). Serie de Correlación Geológica 17: 375-380. S.M. Tucumán.

Astini, R.A.; Dávila, F.M.; Collo, G.; Martina, F. 2005. La Formación La Aguadita (Ordovícico medio-superior): Su implicancia en la evolución temprana del Famatina y como parte del orógeno Oclóyico en el noroeste argentino. *In* Geología de la Provincia de La Rioja (Precámbrico-Paleozoico inferior) (Dahlquist, J.; Baldo, E.; Alasino, P.; editores). Revista de la Asociación Geológica Argentina, Publicación Especial 8 (Serie D): 67-84.

Astini, R.; Collo, G.; Martina, F. 2007. Ordovician K-bentonites in the upper-plate active margin of Western Gondwana, (Famatina Ranges): stratigraphic and palaeogeographic significance. Gondwana Research 11: 311-325.

Bird, D.K.; Spieler, A.R. 2004. Epidote in Geothermal Systems. *In* Epidotes (Liebscher, A.; Franz, G.; editors). Reviews in Mineralogy and Geochemistry 56: 235-300.

Bozkaya, Ö.; Yalçin, H. 2004. Diagenetic to low-grade metamorphic evolution of clay minerals assemblages in Palaeozoic to early Mesozoic rocks of the Eastern Taurides, Turkey. Clay minerals 39 (4): 481-500. DOI: 10.1180/0009855043940149

Brand, U. 2004. Carbon, oxygen and strontium isotopes in Paleozoic carbonate components: an evaluation of original seawater-chemistry proxies. Chemical Geology 204: 23-44.

Champness, P.E.; Cliff, G.; Lorimer, G.W. 1981. Quantitative analytical electron microscopy. Bulletin de Mineralogie 104: 236-240.

Cliff, G.; Lorimer, G.W. 1975. The quantitative analysis of thin specimens. Journal of Microscopy 103: 203-207.

Collo, G. 2006. Caracterización petrográfica y termobarométrica de las unidades con bajo grado de metamorfismo de la región central de Famatina. Tesis doctoral (Inédito), Universidad Nacional de Córdoba: 263 p.

Collo, G. 2008. Historia diagenético-metamórfica de las unidades cambro-ordovícicas en el Famatina: implicancias en la reconstrucción del ciclo orogénico oclóyico. *In* Congreso Geológico Argentino No. 17: 15-16. Jujuy.

Collo, G.; Astini, R.A. 2008. La Formación Achavil: una unidad diferenciable dentro del basamento metamórfico de bajo grado del Famatina en la región pampeana de los Andes Centrales. Revista de la Asociación Geológica Argentina 63 (3): 344-362.

Collo, G.; Do Campo, M.; Astini, R.A. 2005. Caracterización mineralógica, microestructural e historia posdeposicional de la Formación La Aguadita, Sistema de Famatina, La Rioja, Argentina. Revista Mexicana de Ciencias Geológicas 22 (3): 283-297.

Collo, G.; Dávila, F.M.; Candiani, J.C.; Astini, R.A. 2006. Plegamiento transversal a la deformación oclóyica en rocas pre-ordovícicas del Sistema de Famatina. Revista de la Asociación Geológica Argentina 61 (1): 112-117.

Collo, G.; Astini, R.A.; Cardona, A.; Do Campo, M.D.; Cordani, U. 2008. Edad del metamorfismo de las unidades con bajo grado de la región central del Famatina: La impronta del ciclo orogénico oclóyico. Revista Geológica de Chile 35 (2): 191-213.

Collo, G.; Astini, R.A.; Cawood, P.; Buchan, C.; Pimentel, M. 2009. U-Pb detrital zircon ages and Sm-Nd isotopic features in low-grade metasedimentary rocks of the Famatina belt: implications for late Neoproterozoic-Early Paleozoic evolution of the proto-Andean margin

of Gondwana. Journal of the Geological Society of London 166: 1-17.

Currie, C.A.; Hyndman, R.D. 2006. The thermal structure of subduction zone back arcs. Journal of Geophysical Research 111: B08404. DOI:10.1029/2005JB004024

Dahlquist, J.A.; Pankhurst, R.J.; Rapela, C.W.; Galindo, C.; Alasino, P.H.; Casquet, C.; Fanning, C.M.; Saavedra, J.; Baldo, E.G.; González-Casado, J. 2005. New SHRIMP ages in the Sierra de Famatina, NW Argentina: implications for the Famatinian Orogen. *In* Gondwana 12 Conference: p. 123. Mendoza.

Dahlquist, J.A.; Pankhurst, R.J.; Rapela, C.W.; Galindo, C.; Alasino, P.; Fanning, C.M.; Saavedra, J.; Baldo, E.; 2008. New shrimp U-Pb data from the famatina complex: constraining Early-Mid Ordovician Famatinian magmatism in the Sierras Pampeanas, Argentina. Geologica Acta 6 (4): 319-333.

Dávila, F.M. 2003. Transecta Estratigráfica-Estructural a los 28º30'-28º45' de Latitud sur, Sierra de Famatina, Provincia de La Rioja Argentina. Tesis doctoral (Inédito), Universidad Nacional de Córdoba: 516 p.

Dávila, F.M.; Astini, R.A. 2007. Cenozoic provenance history of synorogenic conglomerates in western Argentina (Famatina belt): implications for central Andean foreland development. Geological Society of America 119 (4): 609-622.

Dávila, F.M.; Astini, R.A.; Schmidt, C. 2003. Unraveling 470 m.y. of shortening in the Central Andes and documentation of Type 0 folding. Geology 31: 275-278.

Delpino, S.H.; Bjerg, E. A.; Ferracutti, G.R.; Mogessie, A. 2007. Counterclockwise tectonometamorphic evolution of the Pringles Metamorphic Complex, Sierras Pampeanas of San Luis (Argentina). Journal of South America Earth Science 23: 147-175.

Ernst, W.G. 1963. Significance of phengitic micas from low-grade schists. American Mineralogist 48: 1357-1373.

Fernández, C.; Becchio, R.; Castro, A.; Viramonte, J.M.; Moreno-Ventas, I.; Corretgé, L.G. 2008. Massive generation of atypical ferrosilicic magmas along the Gondwana active margin: Implications for cold plumes and back-arc magma generation. Gondwana Research 14: 451-473.

Gaudin, A.; Buatier, M.D.; Beaufort, D.; Petit, S.; Grauby, O.; Decarreau, A. 2005. Characterization and origin of Fe^{3+}-montmorillonite in deep-water calcareous sediments (Pacific Ocean, Costa Rica margin). Clays and Clay Minerals 53 (5): 452-465. DOI: 10.1346/CCMN.2005.0530503

Guidotti, C.V.; Sassi, F.P. 1986. Classification and Correlation of Metamorphic Facies Series by Means of Muscovite b_0 data from Low-Grade Metapelites. Neues Jahrbuch für Mineralogie Abhandlungen 153 (3): 363-380.

Guidotti, C.V.; Yates, M.G.; Dyar, M.D.; Taylor, M.E.; 1994. Petrogenetic implications of the FeH content of muscovite in pelitic schists. American Mineralogist 79: 793-795.

Hillier, S.; Velde, B. 1991. Octahedral occupancy and chemical composition of diagenetic (low-temperature) chlorites. Clay Minerals 26 (2): 149-168.

Hyndman, R.D.; Currie, C.A.; Mazzotti, S.P. 2005. Subduction zone backarcs, mobile belts, and orogenic heat. GSA Today 15 (2): 4-10. DOI:10.1130/1052-5173(2005)015,4:SZBMBA.2.0.co;2

Jiang, W.; Peacor, D.R. 1994. Prograde transitions of corrensite and chlorite in low-grade pelitic rocks from the Gaspe Peninsula, Quebec. Clays and Clay Minerals 42 (5): 497-517.

Kisch, H.J.; Sassi, R.; Sassi, F.P. 2006. The b_0 lattice parameter and chemistry of phengites from HP/LT metapelites. European Journal of Mineralogy 18 (2): 207-222. DOI: 10.1127/0935-1221/2006/0018-0207

Knipe, R.J. 1981. The interaction between deformation and metamorphism in slates. Tectonophysics 78: 249-272.

Laird, J. 1988. Chlorites: Metamorphic petrology. *In* Hydrous Phyllosilicates (exclusive of micas) (Bailey, S.W.; editor), MSA (Mineralogical Society of America) Reviews in Mineralogy 19: 405-453.

Livi, K.J.T.; Christidis, G.E.; Árkai, P.; Veblen, D.R. 2008. White mica domain formation: A model for paragonite, margarite, and muscovite formation during prograde metamorphism. American Mineralogist 93 (4): 520-527. DOI: 10.2138/am.2008.2662

Mángano, M.G.; Buatois, L.A. 1994. Estratigrafía y ambiente de sedimentación de la Formación Suri en los alrededores del río Chaschuil, Ordovícico del Sistema del Famatina, noroeste argentino. Revista de la Asociación Argentina de Sedimentología 1: 143-169.

Massonne, H.J.; Schreyer, W. 1987. Phengite geobarometry based on the limiting assemblage with K-feldspar, pholgopite and quartz. Contributions to Mineralogy and Petrology 96: 212-224.

Massone, H.J.; Szpurka, Z. 1997. Thermodynamic properties of white micas on the basis of high-pressure experiments in the systems K_2O-MgO-Al_2O_3-SiO_2-H_2O and K_2O-FeO-Al_2O_3-SiO_2-H_2O. Lithos 41: 229-250.

Merriman, R.J.; Peacor, D.R. 1999. Very low-grade metapelites: mineralogy, microfabrics and measuring reaction progress. *In* Low-Grade Metamorphism (Frey, M.; Robinson, D.; editors), Blackwell Sciences, Oxford: 10-60.

Moore, D.M.; Reynolds, R.C. 1997. X-Ray diffraction and the identification and analysis of clay minerals. Oxford University Press, New York: 378 p.

Nieto, F. 1997. Chemical composition of metapelitic chlorites: X-ray diffraction and optical property approach. European Journal of Mineralogy 9: 829-841.

Nieto, F.; Peacor, D.R. 1993. Regional retrograde alteration of prograde lower grade hydrated assemblages. Terra Abstract: 419.

Nieto, F.; Abad, I. 2007. Clay-slate evolution. Onset of metamorphism. Invited Lectures, Euroclay: 34-41.

Nieto, F.; Velila, N.; Peacor, D.; Ortega Huertas, M. 1994. Regional retrograde alteration of sub-greenschist facies chlorite to smectite. Contributions to Mineralogy and Petrology 115: 243-252.

Nieto, F.; Ortega-Huertas, M.; Peacor, D.R.; Arostegui, J.; 1996. Evolution of illite/smectite from early diagenesis through incipient metamorphism in sediments of the Basque-Cantabrian Basin. Clays and Clay Minerals 44 (3): 304-323.

Nieto, F.; Mata, P.M.; Bauluz, B.; Giorgetti, G.; Árkai, P.; Peacor, D.R. 2005. Retrograde diagenesis, a widespread process on a regional scale. Clay minerals 40 (1): 93-104.

Pankhurst, R.J.; Rapela, C.W.; Fanning, C.M. 2000. Age and origin of coeval TTG, I- and S- type granites in the Famatinian belt of NW Argentina. Transaction of the Royal Society Edinburgh Earth Sciences 91: 151-168.

Passchier, C.; Trouw, R.A.J. 1998. Microtectonics. Springer: 289. New York.

Rapela, C.W.; Pankhurst, R.J.; Casquet, C.; Baldo, E.; Saavedra, J.; Galindo, C. 1998. Early evolution of the Proto-Andean margin of South America. Geology 26: 707-710.

Rapela, C.W.; Pankhurst, R.J.; Casquet, C.; Fanning, C.M.; Baldo, E.G.; Gonzalez-Casado, J.M.; Galindo, C.; Dahlquist, J. 2007. The Rio de La Plata craton and the assembly of SW Gondwana, Earth-Science Reviews 83 (1-2): 49-82.

Sassi, F.P.; Scolari, A. 1974. The b_0 value of the potassic white mica as a barometric indicator in low-grade metamorphism of pelitic schists. Contribution of Mineralogy and Petrology 45: 143-152.

Schoonen, M.A.A. 2004. Mechanisms of sedimentary pyrite formation. *In* Sulfur biogeochemistry-Past and present: Boulder, Colorado (Amend, J.P.; Edwards, K.J.; Lyons, T.W.; editors), Geological Society of America Special Paper 379: 117-134.

Steenken, A.;Wemmer, K.; López de Luchi, M.G.; Siegesmund, S.; Pawlig, S. 2004. Crustal Provenace and Cooling of the Basement Complexes of the Sierra de San Luis: An insight Into the Tectonic History of the Proto-Andean Margin of Gondwana. Gondwana Research 7 (4): 1171-1195.

Steenken, A.; Siegesmund, S.; López de Luchi, M.G.; Feri, R.; Wemmer, K. 2006. Neoproterozoic to Early Palaeozoic events in the Sierra de San Luis: implications for the Famatinian geodynamics in the Eastern Sierras Pampeanas (Argentina). Journal of the Geological Society 163: 965-982.

Toselli, A.J.; Weber, K. 1982. Anquimetamorfismo en rocas del Paleozoico inferior en el noroeste de Argentina. Valor de la cristalinidad de la illita como índice. Acta Geológica Lilloana 16: 187-200.

Vaughan, A.P.M.; Pankhurst, R.J. 2008. Tectonic overview of the West Gondwana margin. Gondwana Research 13: 150-162.

Verdecchia, S. 2009. Las metamorfitas de baja presión vinculadas al arco magmático famatiniano: Las unidades metamórficas de la Quebrada de La Cébila y el borde oriental del Velasco. Provincia de La Rioja, Argentina, Universidad Nacional de Córdoba, Tesis doctoral: 312 p.

Warr, L.N.; Rice, A.H.N. 1994. Interlaboratory standardization and calibration of clay mineral cristallinity and cristallite size data. Journal of Metamorphic Geology 12: 141-152.

Whitney, D.L.; Evans, B.W. 2010. Abbreviations for names of rock-forming minerals. American mineralogist 95: 185-187.

Zimmerman, U.; Esteban, S.B. 2002. Provenance and facies of the Volcancito Formation, Famatina Range (Northwestern Argentina). *In* Congreso Geológico Argentino, No. 15, Actas 1: 786-791. Buenos Aires.

Manuscript received: May 31, 2010; revised/accepted: February 02, 2011; available online: March 23, 2011.

APPENDIX A. CHEMICAL COMPOSITIONS FOR DIOCTAHEDRAL MICAS.

	Si	Al^{IV}	Al^{VI}	Fe	Mg	Mn	Ti	∑ oct	K	Na	Ca	∑ int
La Aguadita Formation												
LAG-1	3.19	0.81	1.73	0.14	0.18	0.00	0.00	2.04	0.89	0.00	0.00	0.89
LAG-2	3.20	0.80	1.70	0.13	0.17	0.00	0.01	2.02	0.91	0.03	0.00	0.94
LD2p-1	3.20	0.80	1.58	0.24	0.20	0.00	0.01	2.04	0.93	0.00	0.01	0.94
LD2p-2	3.20	0.80	1.65	0.16	0.20	0.01	0.01	2.03	0.91	0.01	0.01	0.93
LD2p-3	3.24	0.76	1.63	0.20	0.18	-0.01	0.01	2.02	0.89	0.02	0.00	0.91
LD2p-4	3.35	0.65	1.60	0.17	0.21	0.01	0.01	2.00	0.87	0.02	0.00	0.89
LD2p-5	3.21	0.79	1.65	0.17	0.20	0.00	0.01	2.03	0.92	0.01	0.00	0.93
LD2p-6	3.22	0.78	1.65	0.15	0.19	0.01	0.01	2.02	0.93	0.02	0.00	0.95
LD2p-7	3.30	0.70	1.60	0.20	0.21	0.00	0.01	2.02	0.87	0.01	0.00	0.88
LD2p-8	3.22	0.78	1.62	0.19	0.21	0.00	0.01	2.04	0.90	0.01	0.00	0.91
LD2p-9	3.22	0.78	1.59	0.21	0.22	0.01	0.02	2.04	0.89	0.01	0.00	0.91
LD2p-10	3.22	0.78	1.60	0.21	0.21	0.00	0.01	2.03	0.88	0.02	0.01	0.92
LD9p-1*	3.35	0.65	1.64	0.18	0.22	0.00	0.00	2.04	0.80	0.00	0.00	0.80
LD9p-2	3.09	0.91	1.86	0.06	0.08	0.00	0.00	2.01	0.90	0.07	0.00	0.98
LD9p-3*	3.46	0.54	1.49	0.24	0.26	0.00	0.02	2.01	0.78	0.02	0.01	0.81
LD9p-4*	3.38	0.62	1.58	0.20	0.20	0.00	0.02	2.00	0.83	0.02	0.01	0.85
LD9p-5*	3.30	0.70	1.59	0.20	0.23	0.00	0.01	2.04	0.81	0.03	0.01	0.85
LD9p-7	3.12	0.88	1.88	0.05	0.05	0.00	0.02	2.01	0.78	0.12	0.00	0.90
LD9p-8*	3.29	0.71	1.59	0.19	0.24	0.01	0.03	2.05	0.81	0.01	0.00	0.82
LD9p-9	3.11	0.89	1.61	0.25	0.12	0.00	0.06	2.04	0.87	0.03	0.00	0.90
LD9p-10	3.21	0.79	1.60	0.21	0.20	0.00	0.03	2.04	0.86	0.02	0.00	0.89
LD9p-11	3.08	0.92	1.89	0.06	0.06	0.00	0.01	2.02	0.88	0.03	0.00	0.91
LD9p-12	3.21	0.79	1.69	0.17	0.16	0.01	0.01	2.04	0.85	0.01	0.00	0.86
LD9p-13	3.15	0.85	1.84	0.13	0.04	0.00	0.00	2.00	0.90	0.01	-0.01	0.91
LD9p-14	3.23	0.77	1.71	0.16	0.14	0.00	0.01	2.02	0.87	0.03	0.00	0.89
Achavil Formation												
V5m-1	3.34	0.66	1.48	0.26	0.25	0.01	0.03	2.03	0.94	0.00	0.00	0.94
V5m-2	3.35	0.65	1.43	0.33	0.26	0.00	0.03	2.04	0.85	0.05	0.01	0.91
V5m-3	3.41	0.59	1.48	0.24	0.24	0.00	0.03	2.00	0.90	0.01	0.01	0.91
V5m-4	3.27	0.73	1.45	0.36	0.20	0.01	0.02	2.04	1.00	0.00	0.00	1.00
V5m-5	3.26	0.74	1.38	0.40	0.23	0.01	0.02	2.05	1.00	0.01	0.00	1.01
V5m-6	3.27	0.73	1.42	0.38	0.21	0.01	0.02	2.03	1.00	0.01	0.00	1.01
V5m-7	3.26	0.74	1.44	0.37	0.21	0.00	0.02	2.05	0.98	0.00	0.00	0.98
V5m-8	3.23	0.77	1.38	0.42	0.23	0.01	0.03	2.06	0.97	0.03	0.00	0.99
V5m-9	3.16	0.84	1.77	0.13	0.08	0.00	0.02	2.00	0.88	0.09	0.00	0.96
V5m-10	3.28	0.72	1.63	0.20	0.20	0.01	0.02	2.06	0.81	0.03	0.01	0.84
V5m-11*	3.28	0.72	1.70	0.15	0.17	0.00	0.02	2.04	0.80	0.03	0.00	0.83
V12-1	3.23	0.77	1.50	0.26	0.21	0.01	0.08	2.05	0.87	0.01	0.00	0.88
V12-2	3.17	0.83	1.69	0.18	0.11	0.01	0.03	2.01	0.94	0.02	0.00	0.96

Appendix A continued.

	Si	Al^{IV}	Al^{VI}	Fe	Mg	Mn	Ti	∑ oct	K	Na	Ca	∑ int
Achavil Formation												
V12-3	3.19	0.81	1.52	0.29	0.17	0.01	0.05	2.04	0.94	0.03	0.00	0.96
V12-4	3.26	0.74	1.50	0.28	0.23	0.00	0.03	2.04	0.92	0.04	0.00	0.96
V12-5	3.25	0.75	1.49	0.29	0.24	0.01	0.02	2.05	0.95	0.03	0.00	0.98
V12-6	3.25	0.75	1.51	0.27	0.23	0.00	0.02	2.04	0.96	0.03	0.00	0.99
V12-7	3.35	0.65	1.59	0.19	0.26	0.00	0.01	2.04	0.85	0.00	0.01	0.86
V12-8	3.08	0.92	1.85	0.08	0.06	0.00	0.02	2.02	0.87	0.08	0.00	0.95
V12-9*	3.41	0.59	1.61	0.15	0.23	0.00	0.03	2.01	0.80	0.02	0.01	0.82
V12-10	3.17	0.83	1.69	0.15	0.16	0.00	0.03	2.03	0.92	0.03	0.00	0.95
V12-11	3.09	0.91	1.67	0.22	0.09	0.00	0.05	2.04	0.90	0.05	0.00	0.95
V15-1	3.18	0.82	1.60	0.23	0.12	0.00	0.04	2.00	1.01	0.01	0.00	1.02
V15-2	3.23	0.77	1.59	0.22	0.16	0.00	0.03	2.00	0.99	0.03	0.00	1.01
V15-3	3.14	0.86	1.76	0.12	0.13	0.00	0.01	2.03	0.91	0.06	0.00	0.97
V15-4	3.26	0.74	1.39	0.36	0.27	0.01	0.03	2.06	0.96	0.03	0.00	0.99
V15-5	3.05	0.95	1.84	0.06	0.06	0.00	0.04	2.01	0.89	0.09	0.00	0.97
V15-6	3.19	0.81	1.71	0.18	0.10	0.01	0.03	2.04	0.75	0.12	0.00	0.86
V15-7	3.19	0.81	1.73	0.14	0.13	0.00	0.01	2.01	0.90	0.05	0.00	0.95
V15-8	3.19	0.81	1.76	0.13	0.12	0.00	0.01	2.01	0.91	0.03	0.00	0.94
V15-9	3.16	0.84	1.75	0.14	0.11	0.00	0.01	2.01	0.92	0.06	0.00	0.98
V15-10	3.19	0.81	1.80	0.11	0.08	0.01	0.01	2.01	0.91	0.01	0.00	0.92
V15-11	3.30	0.70	1.35	0.50	0.18	0.01	0.02	2.05	0.96	0.00	0.00	0.97
V15-12	3.25	0.75	1.70	0.15	0.14	0.00	0.01	2.01	0.90	0.02	0.00	0.92
V15-13	3.16	0.84	1.74	0.11	0.12	0.00	0.03	2.01	0.92	0.03	0.01	0.95
V15-14*	3.24	0.76	1.82	0.09	0.10	0.00	0.01	2.02	0.82	0.01	0.01	0.83
V15-15	3.28	0.72	1.57	0.22	0.21	0.00	0.02	2.02	0.87	0.03	0.03	0.93
V15-16	3.24	0.76	1.67	0.17	0.17	0.00	0.02	2.03	0.90	0.01	0.00	0.91
V15-17*	3.36	0.64	1.55	0.24	0.22	0.00	0.02	2.03	0.85	0.00	0.00	0.85
V15-18*	3.43	0.57	1.55	0.09	0.38	0.00	0.02	2.04	0.84	0.00	0.00	0.84
V15-19	3.42	0.58	1.46	0.22	0.33	0.00	0.02	2.03	0.80	0.11	0.00	0.91
V15-20*	3.37	0.63	1.61	0.23	0.16	0.00	0.02	2.01	0.85	0.00	0.00	0.85
ACH-1	3.37	0.63	1.31	0.36	0.34	0.00	0.02	2.03	0.18	0.78	0.00	0.96
ACH-2	3.17	0.83	1.84	0.09	0.11	0.00	0.00	2.03	0.86	0.00	0.00	0.86
ACH-3	3.16	0.84	1.74	0.12	0.18	0.00	0.00	2.04	0.92	0.00	0.00	0.92
ACH-5	3.20	0.80	1.68	0.14	0.15	0.00	0.03	2.01	0.81	0.12	0.00	0.93
ACH-6	3.16	0.84	1.62	0.18	0.21	0.00	0.04	2.04	0.55	0.39	0.00	0.94
ACH-7*	3.37	0.63	1.50	0.17	0.28	0.00	0.00	1.95	0.61	0.21	0.00	0.82
ACH-8*	3.33	0.67	1.51	0.18	0.26	0.00	0.00	1.94	0.68	0.15	0.00	0.83
546-1	3.18	0.82	1.60	0.25	0.14	0.00	0.04	2.04	0.89	0.05	0.00	0.94
546-3	3.14	0.86	1.81	0.10	0.09	0.00	0.02	2.02	0.88	0.05	0.00	0.93
546-4	3.17	0.83	1.66	0.23	0.15	0.00	0.02	2.06	0.87	0.03	0.01	0.90
546-6	3.24	0.76	1.61	0.20	0.20	0.00	0.03	2.05	0.72	0.17	0.00	0.89

Appendix A continued.

	Si	Al^{IV}	Al^{VI}	Fe	Mg	Mn	Ti	∑ oct	K	Na	Ca	∑ int
Achavil Formation												
546-7	3.14	0.86	1.83	0.10	0.07	0.00	0.01	2.00	0.86	0.08	0.00	0.95
546-11	3.11	0.89	1.79	0.10	0.16	0.00	0.02	2.06	0.85	0.04	0.00	0.88
546-12	3.24	0.76	1.72	0.11	0.17	0.00	0.02	2.02	0.85	0.05	0.00	0.89
Negro Peinado Formation												
NP2-3	3.20	0.80	1.57	0.25	0.16	0.00	0.02	2.00	1.00	0.02	0.00	1.01
NP2-4	3.12	0.88	1.62	0.22	0.11	0.00	0.04	2.00	1.01	0.02	0.00	1.03
NP2-5	3.14	0.86	1.66	0.21	0.12	0.00	0.03	2.02	0.92	0.04	0.00	0.96
NP2-6	3.17	0.83	1.62	0.21	0.17	0.00	0.01	2.02	0.93	0.04	0.00	0.98
NP3-1*	3.17	0.83	1.74	0.16	0.12	0.00	0.02	2.04	0.82	0.02	0.00	0.84
NP3-2	3.25	0.75	1.58	0.23	0.19	0.00	0.02	2.02	0.90	0.01	0.00	0.91
NP3-3	3.27	0.73	1.59	0.22	0.18	0.00	0.01	2.01	0.89	0.05	0.00	0.94
NP3-4	3.33	0.67	1.55	0.25	0.18	0.00	0.02	2.00	0.86	0.03	0.00	0.89
NP3-5	3.19	0.81	1.61	0.23	0.17	0.01	0.02	2.03	0.89	0.04	0.00	0.92
NP3-6	3.14	0.86	1.82	0.06	0.11	0.00	0.03	2.03	0.84	0.04	0.00	0.88
NP3-7	3.15	0.85	1.65	0.21	0.13	0.00	0.03	2.02	0.93	0.03	0.00	0.96
NP3-8	3.21	0.79	1.56	0.26	0.19	0.00	0.02	2.04	0.89	0.03	0.00	0.92
NP3-9	3.22	0.78	1.60	0.24	0.17	0.00	0.02	2.03	0.88	0.03	0.00	0.91
CH73-1	3.09	0.91	1.79	0.11	0.09	0.01	0.03	2.02	0.87	0.07	0.00	0.94
CH73-3	3.18	0.82	1.77	0.11	0.09	0.00	0.03	2.00	0.84	0.07	0.00	0.91
CH73-4	3.06	0.89	1.83	0.11	0.05	0.00	0.02	2.01	0.90	0.08	0.00	0.98
CH73-5	3.11	0.89	1.76	0.12	0.11	0.00	0.03	2.02	0.87	0.07	0.00	0.95
CH73-9	3.11	0.89	1.77	0.12	0.10	0.00	0.02	2.01	0.91	0.06	0.00	0.97
CH64-1	3.15	0.85	1.75	0.11	0.13	0.00	0.02	2.01	0.92	0.05	0.00	0.97
CH64-2	3.16	0.84	1.73	0.14	0.13	0.00	0.02	2.03	0.86	0.06	0.00	0.91
CH64-3	3.29	0.71	1.73	0.12	0.14	0.00	0.01	2.00	0.81	0.05	0.00	0.87
CH64-4	3.12	0.88	1.84	0.05	0.10	0.00	0.02	2.00	0.88	0.07	0.00	0.95
CH64-5	3.14	0.86	1.76	0.10	0.14	0.00	0.01	2.02	0.89	0.04	0.00	0.94
QP3a-3	3.18	0.82	1.64	0.18	0.17	0.00	0.01	2.01	1.01	0.00	0.00	1.01
QP3a-8	3.09	0.91	1.87	0.07	0.05	0.01	0.02	2.00	0.95	0.03	0.00	0.98
QP3a-11	3.09	0.91	1.77	0.12	0.09	0.00	0.02	2.00	0.98	0.03	0.00	1.01
QP3a-13	3.23	0.77	1.61	0.19	0.18	0.01	0.02	2.01	0.90	0.02	0.01	0.93
QP3a-14	3.27	0.73	1.67	0.10	0.20	0.00	0.02	2.00	0.90	0.05	0.00	0.95
QP3a-17	3.33	0.67	1.50	0.21	0.30	0.00	0.01	2.03	0.90	0.03	0.00	0.93
QP3a-18	3.32	0.68	1.42	0.28	0.31	0.00	0.02	2.03	0.91	0.04	0.00	0.95
QP3a-19	3.33	0.67	1.44	0.25	0.32	0.00	0.02	2.03	0.91	0.04	0.00	0.94
QP3a-20	3.26	0.74	1.57	0.19	0.26	0.00	0.01	2.04	0.88	0.03	0.00	0.91
QP3a-21	3.24	0.76	1.66	0.15	0.20	0.00	0.02	2.02	0.88	0.03	0.00	0.91
QP3a-22	3.15	0.85	1.75	0.13	0.14	0.00	0.01	2.03	0.90	0.03	0.00	0.93

Appendix A continued.

	Si	Al^{IV}	Al^{VI}	Fe	Mg	Mn	Ti	∑ oct	K	Na	Ca	∑ int
Negro Peinado Formation												
QP3a-23	3.27	0.73	1.55	0.17	0.23	0.01	0.06	2.01	0.91	0.02	0.00	0.93
QP3a-24	3.21	0.79	1.67	0.13	0.18	0.00	0.02	2.01	0.92	0.03	0.00	0.95
QP3a-25	3.32	0.68	1.62	0.16	0.20	0.01	0.02	2.00	0.89	0.01	0.00	0.90
QP3a-26	3.27	0.73	1.59	0.21	0.18	0.00	0.03	2.01	0.77	0.11	0.01	0.89
QP3a-28	3.25	0.75	1.74	0.13	0.11	0.01	0.02	2.00	0.85	0.02	0.00	0.87
QP3a-29*	3.23	0.77	1.59	0.25	0.20	0.01	0.02	2.06	0.74	0.07	0.01	0.82
QP3a-30	3.39	0.61	1.57	0.18	0.22	0.00	0.02	2.00	0.85	0.03	0.00	0.87
QP3a-31	3.32	0.68	1.64	0.16	0.18	0.00	0.02	2.01	0.84	0.03	0.00	0.87
QP3a-32	3.26	0.74	1.78	0.09	0.11	0.00	0.01	2.00	0.81	0.05	0.00	0.86
CNP-1	3.12	0.88	1.75	0.14	0.11	0.00	0.02	2.03	0.85	0.06	0.00	0.91
CNP-2	3.09	0.91	1.80	0.11	0.07	0.00	0.02	2.01	0.91	0.06	0.00	0.97
CNP-3	3.07	0.93	1.81	0.11	0.07	0.00	0.03	2.02	0.89	0.06	0.00	0.95
CNP-4	3.13	0.87	1.78	0.12	0.08	0.00	0.02	2.01	0.90	0.03	0.00	0.93
CH55-2	3.25	0.75	1.68	0.15	0.15	0.00	0.02	2.00	0.87	0.03	0.00	0.91
517-1	3.22	0.78	1.61	0.23	0.13	0.00	0.02	2.00	0.88	0.07	0.00	0.95
517-2	3.23	0.77	1.62	0.19	0.16	0.01	0.02	2.00	0.94	0.04	0.00	0.97
517-3	3.10	0.90	1.71	0.19	0.10	0.00	0.02	2.02	0.93	0.03	0.00	0.96
517-4	3.09	0.91	1.71	0.19	0.09	0.00	0.02	2.01	0.94	0.04	0.00	0.98
517-5	3.21	0.79	1.71	0.18	0.10	0.00	0.01	2.01	0.82	0.09	0.00	0.90

*: analyses showing illitic substitution.

APPENDIX B. CHEMICAL COMPOSITIONS FOR TRIOCTAHEDRAL MICAS.

	Si	Al^{IV}	Al^{VI}	Fe	Mg	Mn	Ti	∑ oct.	F/FM
La Aguadita Formation									
Lag-1	2.82	1.14	1.36	2.62	1.88	0.10	0.00	5.96	0.58
Lag-2	2.92	1.06	1.29	2.71	1.84	0.09	0.00	5.94	0.60
Lag-3	3.27	0.71	1.50	2.30	1.74	0.09	0.00	5.63	0.57
Lag-4	2.79	1.20	1.29	2.64	1.94	0.10	0.00	5.97	0.58
Lag-5	2.72	1.23	1.28	2.73	1.95	0.10	0.00	6.06	0.58
Lag-6	2.62	1.38	1.42	2.54	1.91	0.11	0.00	5.98	0.57
Lag-7	2.73	1.27	1.35	2.45	2.03	0.12	0.00	5.96	0.55
Lag-8	2.73	1.27	1.35	2.57	1.94	0.09	0.00	5.96	0.57
Lag-9	2.64	1.36	1.35	2.65	1.91	0.09	0.00	6.01	0.58
Lag-10	2.69	1.31	1.38	2.59	1.89	0.11	0.00	5.97	0.58
Lag-11	2.79	1.21	1.33	2.76	1.73	0.11	0.00	5.94	0.61
LD9a-1	2.81	1.17	1.32	2.35	2.22	0.07	0.00	5.96	0.51
LD9a-2	2.71	1.24	1.32	2.47	2.20	0.06	0.00	6.06	0.53
LD9p-1	3.21	0.76	1.51	2.47	1.64	0.06	0.01	5.69	0.60
LD9p-2	3.08	0.88	1.39	2.82	1.55	0.07	0.00	5.83	0.65
Achavil Formation									
V12-1	2.71	1.28	1.54	2.81	1.49	0.05	0.00	5.88	0.65
V12-2	2.68	1.27	1.20	2.84	2.06	0.03	0.01	6.12	0.58
V12-3	2.62	1.35	1.24	2.83	2.00	0.03	0.01	6.11	0.59
V12-4	2.69	1.26	1.29	2.78	1.97	0.02	0.01	6.07	0.59
V15-1	2.95	1.03	1.20	2.66	1.98	0.06	0.03	5.92	0.57
V15-2	2.95	1.02	1.16	2.68	2.02	0.05	0.04	5.95	0.57
V15-3	3.14	0.82	1.58	2.58	1.47	0.05	0.00	5.70	0.64
V15-4	2.90	1.12	1.46	2.63	1.65	0.06	0.00	5.80	0.62
V15-5	2.82	1.19	1.16	2.72	2.06	0.03	0.01	5.98	0.57
V15-6	2.76	1.23	1.07	2.81	1.55	0.06	0.31	5.80	0.65
V15-7	2.98	0.99	1.08	2.61	2.03	0.06	0.12	5.90	0.56
V15-8	2.89	1.09	1.43	2.33	1.97	0.05	0.05	5.83	0.54
V15-9	2.86	1.14	1.38	2.35	2.09	0.05	0.00	5.88	0.53
V15-10	2.80	1.15	1.57	2.46	1.81	0.05	0.00	5.89	0.58
V15-11	3.29	0.68	1.12	1.67	2.97	0.03	0.03	5.82	0.36
V15-14	2.98	1.00	1.56	2.28	1.88	0.05	0.00	5.76	0.55
V15-15	3.26	0.72	1.60	2.19	1.77	0.04	0.00	5.60	0.55
V15-16	2.88	1.12	1.23	2.24	1.68	0.04	0.38	5.57	0.57
V15-17	2.91	1.06	1.56	2.41	1.79	0.04	0.00	5.80	0.57
546-1	2.73	1.23	1.43	2.20	2.31	0.03	0.00	5.97	0.49
546-2	2.62	1.33	1.34	2.29	2.42	0.04	0.02	6.09	0.49
546-3	2.80	1.15	1.45	2.15	2.29	0.03	0.02	5.94	0.48
546-4	2.67	1.28	1.43	2.25	2.30	0.03	0.00	6.02	0.49
546-5	2.65	1.33	1.41	2.22	2.34	0.03	0.00	6.01	0.49
546-6	2.61	1.38	1.37	2.14	2.49	0.03	0.00	6.04	0.46
546-7	2.67	1.32	1.37	2.10	2.51	0.03	0.00	6.01	0.45
546-8	2.63	1.37	1.22	2.09	2.40	0.03	0.16	5.91	0.47

Appendix B continued.

	Si	Al^{IV}	Al^{VI}	Fe	Mg	Mn	Ti	∑ oct.	F/FM
Negro Peinado Formation									
NP2-1	2.67	1.28	1.22	2.10	2.47	0.07	0.13	5.99	0.46
NP2-2	2.65	1.31	1.29	2.05	2.65	0.07	0.00	6.07	0.44
NP2-3	2.81	1.15	1.40	1.93	2.54	0.07	0.00	5.95	0.43
NP2-4	2.77	1.20	1.49	1.91	2.43	0.07	0.00	5.90	0.44
NP2-5	3.03	0.92	2.03	1.53	1.93	0.04	0.00	5.53	0.44
NP2-6	2.75	1.21	1.48	2.18	2.21	0.06	0.01	5.94	0.50
NP2-7	2.75	1.22	1.37	2.20	2.30	0.07	0.01	5.96	0.49
NP2-8	2.99	0.97	1.49	2.06	2.19	0.07	0.00	5.82	0.48
NP2-9	2.96	1.01	1.47	2.06	2.22	0.07	0.01	5.83	0.48
NP2-10	2.74	1.22	1.40	2.16	2.34	0.09	0.00	5.99	0.48
NP3-1	2.68	1.28	1.34	2.18	2.47	0.05	0.00	6.04	0.47
NP3-2	2.67	1.28	1.26	2.34	2.44	0.06	0.00	6.10	0.49
CH73-1	2.60	1.39	1.42	2.54	2.00	0.05	0.00	6.01	0.56
CH73-2	2.63	1.38	1.51	2.40	1.95	0.05	0.01	5.91	0.55
CH73-3	2.63	1.37	1.49	2.31	2.09	0.05	0.00	5.94	0.53
CH73-4	2.63	1.36	1.58	2.30	1.96	0.07	0.00	5.91	0.54
CH73-5	2.60	1.37	1.49	2.38	2.08	0.04	0.00	5.99	0.53
CH73-6	2.53	1.47	1.48	2.38	2.10	0.04	0.00	6.00	0.53
CH73-7	2.55	1.45	1.40	2.46	2.11	0.06	0.00	6.03	0.54
CH73-8	2.62	1.36	1.40	2.41	2.17	0.05	0.00	6.02	0.53
CH73-9	2.56	1.42	1.48	2.46	2.03	0.04	0.00	6.01	0.55
CH73-10	2.50	1.50	1.46	2.40	2.09	0.05	0.00	6.02	0.53
CH73-11	2.56	1.44	1.45	2.42	2.07	0.05	0.00	5.99	0.54
CH73-12	2.61	1.39	1.48	2.40	2.02	0.05	0.00	5.95	0.54
CH73-13	2.58	1.39	1.46	2.47	2.04	0.06	0.00	6.02	0.55
CH73-14	2.59	1.41	1.45	2.35	2.13	0.05	0.00	5.98	0.52
CH73-15	2.54	1.46	1.38	2.49	2.14	0.04	0.00	6.04	0.54
CH73-16	2.58	1.42	1.44	2.45	2.10	0.00	0.00	5.99	0.54
CH73-17	2.55	1.45	1.45	2.41	2.10	0.04	0.00	6.00	0.53
CH73-18	2.56	1.42	1.44	2.42	2.12	0.04	0.00	6.03	0.53
CH73-19	2.55	1.44	1.43	2.50	2.07	0.03	0.00	6.04	0.55
CH64-1	2.72	1.27	1.42	2.42	2.07	0.02	0.00	5.94	0.54
CH64-2	2.79	1.20	1.40	2.35	2.13	0.03	0.01	5.92	0.52
CH64-3	2.94	1.02	2.01	1.91	1.65	0.02	0.00	5.59	0.54
CH64-4	2.68	1.28	1.37	2.51	2.13	0.03	0.00	6.03	0.54
CH64-5	2.69	1.28	1.41	2.39	2.12	0.03	0.01	5.97	0.53
CH64-6	2.84	1.16	1.65	2.10	1.97	0.03	0.00	5.75	0.52
CH64-7	2.86	1.12	1.38	2.46	2.07	0.00	0.00	5.91	0.54
CH64-9	2.97	1.00	1.48	2.37	1.94	0.03	0.00	5.81	0.55
CH64-10	2.72	1.23	1.34	2.30	2.37	0.02	0.01	6.03	0.49
CH64-11	2.65	1.34	1.37	2.32	2.28	0.02	0.00	6.00	0.50
CH64-12	2.67	1.32	1.32	2.35	2.32	0.03	0.00	6.02	0.50

Appendix B continued.

	Si	Al^{IV}	Al^{VI}	Fe	Mg	Mn	Ti	∑ oct.	F/FM
Negro Peinado Formation									
CH64-13	2.75	1.23	1.49	2.18	2.18	0.03	0.01	5.89	0.50
CH64-14	2.70	1.28	1.34	2.36	2.28	0.02	0.00	6.01	0.51
CH64-15	2.71	1.27	1.36	2.29	2.30	0.03	0.00	5.99	0.50
CH64-16	2.89	1.10	1.46	2.25	2.07	0.03	0.00	5.82	0.52
CH64-17	2.80	1.15	1.55	2.25	2.03	0.02	0.01	5.87	0.53
CH64-18	2.68	1.30	1.36	2.34	2.27	0.03	0.00	6.00	0.51
CH64-19	2.61	1.39	1.39	2.34	2.25	0.03	0.00	6.00	0.51
CH64-20	2.87	1.10	1.73	2.08	1.91	0.02	0.00	5.75	0.52
CH64-22	2.70	1.27	1.35	2.30	2.33	0.03	0.00	6.01	0.50
CH64-23	2.73	1.25	1.47	2.28	2.15	0.03	0.00	5.93	0.52
QP3a-1	2.70	1.26	1.35	2.66	1.93	0.07	0.01	6.02	0.58
QP3a-2	2.72	1.24	1.46	2.58	1.85	0.07	0.00	5.96	0.58
QP3a-3	2.67	1.31	1.38	2.62	1.92	0.07	0.01	6.00	0.58
QP3a-5	2.68	1.32	1.45	2.50	1.93	0.06	0.00	5.94	0.57
QP3a-6	2.98	0.97	1.43	2.72	1.63	0.07	0.00	5.86	0.63
QP3a-7	2.72	1.29	1.28	2.91	1.71	0.06	0.00	5.97	0.63
QP3a-8	2.63	1.34	1.24	3.03	1.78	0.07	0.00	6.12	0.63
QP3a-9	2.62	1.37	1.27	2.88	1.82	0.07	0.01	6.06	0.61
QP3a-10	2.74	1.27	1.33	2.80	1.77	0.07	0.00	5.97	0.61
QP3a-11	2.84	1.15	1.38	2.75	1.69	0.06	0.01	5.90	0.62
QP3a-12	2.73	1.25	1.32	2.86	1.73	0.08	0.00	5.99	0.62
QP3a-13	2.69	1.30	1.30	2.87	1.76	0.08	0.00	6.02	0.62
QP3a-14	2.76	1.22	1.37	2.77	1.75	0.06	0.01	5.96	0.61
QP3a-15	2.65	1.32	1.28	2.91	1.80	0.08	0.01	6.07	0.62
QP3a-16	2.65	1.35	1.42	2.49	1.98	0.07	0.01	5.96	0.56
QP3a-18	2.66	1.33	1.40	2.53	1.97	0.07	0.01	5.97	0.56
QP3a-19	2.88	1.12	1.50	2.37	1.88	0.06	0.00	5.81	0.56
QP3a-21	2.84	1.15	1.44	2.39	1.98	0.06	0.00	5.87	0.55
QP3a-22	2.67	1.33	1.36	2.49	2.05	0.07	0.01	5.99	0.55
CNP-1	2.63	1.35	1.53	2.41	1.96	0.04	0.01	5.95	0.55
CNP-2	3.18	0.82	1.64	2.09	1.85	0.00	0.00	5.59	0.53
CH55-1	2.71	1.26	1.40	2.66	1.87	0.04	0.01	5.98	0.59
CH55-2	2.64	1.33	1.39	2.74	1.85	0.04	0.01	6.03	0.60
CH55-3	2.65	1.31	1.36	2.76	1.89	0.04	0.00	6.05	0.59
CH55-4	2.70	1.28	1.44	2.62	1.85	0.04	0.00	5.96	0.59
517-1	2.67	1.31	1.41	2.38	2.12	0.07	0.00	5.98	0.53
517-2	2.59	1.36	1.35	2.47	2.22	0.08	0.00	6.11	0.53
517-3	2.61	1.36	1.35	2.44	2.17	0.09	0.01	6.06	0.53
517-4	2.64	1.36	1.48	2.05	2.33	0.08	0.00	5.94	0.47